

The importance of turbulent ocean-sea ice nutrient exchanges for simulation of ice algal biomass and production with CICE6.1 and Icepack 1.2

Pedro Duarte¹, Philipp Assmy¹, Karley Campbell^{2,3}, Arild Sundfjord¹

¹ Norwegian Polar Institute, Fram Centre, Tromsø, Norway

² Department of Arctic and Marine Biology, UiT The Arctic University of Norway, Norway

³ Bristol Glaciology Centre, University of Bristol, UK

Correspondence to: Pedro Duarte (Pedro.Duarte@npolar.no)

Abstract. Different sea-ice models apply unique approaches in the computation of nutrient diffusion between the ocean and the ice bottom, which are generally decoupled from the calculation of turbulent ~~momentum and~~ heat flux. Often, a simple molecular diffusion formulation is used. We argue that nutrient transfer from the ocean to sea ice should be as consistent as possible with ~~momentum and~~ heat transfer, since all these fluxes respond to varying forcing in a similar fashion. We hypothesize that biogeochemical models which do not consider such turbulent nutrient exchanges between the ocean and the sea-ice, despite considering brine drainage and bulk exchanges through ice freezing/melting, may underestimate bottom-ice algal production. The Los Alamos Sea Ice Model (CICE + Icepack) was used to test this hypothesis by comparing simulations without and with diffusion of nutrients across sea-ice bottom dependent on velocity-shear, implemented in a way that is consistent with turbulent ~~momentum and~~ heat exchanges. Simulation results support the hypothesis, showing a significant enhancement of ice algal production and biomass when nutrient limitation was relieved by bottom-ice turbulent exchange. Our results emphasize the potentially critical role of turbulent exchanges to sea ice algal blooms, and the importance of thus properly representing them in biogeochemical models. The relevance of this becomes even more apparent considering ongoing trends in the Arctic Ocean, with a predictable shift from light to nutrient limited growth of ice algae earlier in the spring, as the sea ice becomes more fractured and thinner with a larger fraction of young ice with thin snow cover.

1 Introduction

Momentum, heat and mass fluxes between the ocean and the sea-ice are of utmost importance to predict sea-ice motion, thermodynamics, and biogeochemistry. ~~Considering the interlinks between these processes one would expect that sea ice models used a common approach to compute them, notwithstanding their obvious specificities.~~ However, when we look at models released over the last decades, we find not only inter-model differences in the physical concepts used to describe the processes responsible for some of the above fluxes, but also intra-model differences in the approaches used in calculating, for example, heat and mass fluxes. In this work we will focus on the differences related with the vertical diffusion of tracers

31 between the water column and the bottom-ice and attempt to explore their consequences on nutrient limitation for sea-ice algal
32 growth.

33 ~~From this assessment one~~ We may divide the ocean-ice exchange processes of existing biogeochemical models into those
34 related to: (i) entrapment during freezing; (ii) flushing and release during melting; (iii) brine gravity drainage, driven by density
35 instability, parameterized as either a diffusive or a convective process; and (v) turbulent diffusion at
36 the interface between the ocean and the ice induced by velocity shear – the latter process being the focus of this study (e.g.
37 Arrigo et al., 1993 and references therein; Jin et al., 2006; McPhee, 2008; Notz and Worster, 2009; Turner et al., 2013; Tedesco
38 and Vichi, 2010, 2019; Jeffery et al., 2011; Vancoppenolle et al., 2013)~~(e.g. Arrigo et al., 1993 and references therein; Notz~~
39 ~~and Worster, 2009; McPhee, 2008; Turner et al., 2013).~~

40 ~~The most common processes found in the literature to model nutrient exchanges between the water and the sea ice are based~~
41 ~~on entrapment during freezing, release during melting and brine transport (e.g. Arrigo et al., 1993; Jin et al., 2006; Tedesco~~
42 ~~and Vichi, 2010, 2019; Jeffery et al., 2011; Vancoppenolle et al., 2013).~~ These processes are considered in several sea ice
43 models. Arrigo et al. (1993) distinguished nutrient exchanges resulting from gravity drainage in brine channels, from brine
44 convection in the skeletal layer, dependent on the ice growth rate. These brine fluxes were used to calculate nutrient exchanges
45 as a diffusive process. Lavoie et al. (2005) also calculated nutrient exchanges as a diffusive process. Jin et al. (2006; 2008)
46 computed nutrient fluxes across the bottom layer as an advection process dependent on ice growth rate and based on
47 Wakatsuchi and Ono (1983). Molecular diffusion was also considered. More recently, other authors have integrated
48 formulations of “enhanced diffusion” (Vancoppenolle et al., 2010; Jeffery et al., 2011) or convection (Turner et al., 2013),
49 based on hydrostatic instability of brine density profiles, to compute brine gravity drainage and tracer exchange within the ice
50 and between the ice and the sea water. Comparisons between salt dynamics in growing sea ice with salinity measurements
51 showed that convective Rayleigh number-based parameterizations (e.g. Wells et al., 2011), such as the one by Turner et al.
52 (2013), outperform diffusive and simple convective formulations (Thomas et al., 2020).

53 Interestingly, ~~the calculation of momentum and~~ heat exchange is often calculated differently versus from salinity in models ~~is~~
54 ~~often mismatched~~. In the case of the former ~~two~~, typically, a transfer mechanism (turbulent or not) at the interface between the
55 ocean and the sea ice is not dependent on any type of brine exchange. In the case of salinity, such a mechanism is not considered
56 (e.g. Vancoppenolle et al., 2007; Turner et al., 2013). Presumably, such differences result from the relative importance of
57 various physical processes for different tracers. ~~Momentum and h~~Heat transfer between the ice and the water ~~are~~ is a
58 fundamental mechanisms in explaining sea-ice ~~dynamics and~~ thermodynamics, irrespective of brine exchanges. ~~However~~ On
59 the other hand, ice desalination depends mostly on brine gravity drainage and flushing during melting (Notz and Worster,
60 2009).

61 Vertical convective mixing of nutrients under the sea ice may result from brine rejection and/or drainage from the sea ice (Lake
62 and Lewis, 1970; Niedrauer and Martin, 1979; Reeburgh, 1984) and from turbulence due to shear instabilities generated by
63 drag at the interface between the ocean and the sea ice (Gosselin et al., 1985; Cota et al., 1987; Carmack, 1986), internal waves
64 and topographical features (Ingram et al., 1989; Dalman et al., 2019). Gosselin et al. (1985) and Cota et al. (1987) stressed the

65 significance of tidally induced mixing in supplying nutrients to sympagic algae. Biological demand for silicic acid (hereafter
 66 abbreviated as silicate) and nitrate is limited by the physical supply (Cota and Horne, 1989; Cota and Sullivan, 1990). ~~Vertical~~
 67 ~~nutrient fluxes between the water and the bottom ice can be calculated from:~~

$$68 \quad F_e = -K_z \frac{\Delta C}{\Delta z}, \quad (1)$$

69 where K_z is the vertical eddy diffusivity ($\text{m}^2 \text{d}^{-1}$) and ΔC is the difference in nutrient concentration (mmol m^{-3}) over the vertical
 70 distance Δz (m) (Cota et al., 1987).

71 The analysis Table 1 summarizes of several models published over the last decades and their approaches to calculate tracer
 72 diffusion— across the ice-ocean interface shows that Some-some models do not consider this process or limit it to molecular
 73 diffusion. Other models consider turbulent exchanges parameterized as a function of the Rayleigh number, calculated from
 74 brine vertical density gradients. Only one of the sampled models (Mortenson et al., 2017) uses a parameterization based on
 75 friction velocity.

76 ~~From this assessment one may divide the ocean ice exchange processes of existing biogeochemical models into those related~~
 77 ~~to: (i) entrapment during freezing; (ii) flushing and release during melting; (iii) brine gravity drainage, driven by density~~
 78 ~~instability, parameterized as either a diffusive or a convective process; (iv) molecular diffusion; (v) turbulent diffusion at the~~
 79 ~~interface between the ocean and the ice induced by velocity shear—the focus of this study.~~ In the absence of ice growth and
 80 when brine gravity drainage is limited, diffusive nutrient exchanges between the ocean and the ice have the capacity to limit
 81 primary production. This limitation will be alleviated in the presence of a turbulent exchange mechanism. We argue that
 82 nutrient transfer at the interface between the ocean and the sea ice should be as consistent as possible with ~~momentum and~~
 83 heat transfer since all these fluxes are closely linked. We hypothesize that models which do not consider the role of current
 84 velocity shear on turbulent nutrient exchanges between the ocean and the sea-ice may underestimate bottom-ice algal
 85 production. ~~Such underestimation will bias the role of sea ice algae in ice associated food webs and ecosystem services, such~~
 86 ~~as carbon dioxide exchanges and their climate feedbacks.~~

87 To test the above hypothesis, we use a 1D vertically resolved model and contrast results using the default diffusion
 88 parameterization and a “turbulent” parameterization analogous to that of ~~momentum and~~ heat transfer, at the interface between
 89 the ocean and the sea ice, based on McPhee (2008).

90

91 Table 1. Model parameterizations used/proposed by different authors to compute diffusion of tracers. The only example based on
 92 friction velocity is that of Mortenson et al. (2017). “None” is used when exchange processes depend solely on ice growth/melting.

Source	Type of diffusion	Associated model
Cota et al. (1987)	Eddy diffusion	-
Arrigo et al. (1993)	Diffusion based on brine fluxes	A simulated Antarctic fast ice ecosystem
Lavoie et al. (2005)	Molecular diffusion ($1 \cdot 10^{-9} \text{ m}^2 \text{ s}^{-1}$)	Ice algal modelling of the Arctic in Resolute Passage, Canadian archipelago.

Jin et al. (2006; 2008)	Molecular diffusion according to the authors but using a diffusion coefficient ($1.0 \cdot 10^{-5} \text{ m}^2 \text{ s}^{-1}$) that is 4 orders of magnitude higher than molecular diffusion of salt [$1.0 \cdot 10^{-9} \text{ m}^2 \text{ s}^{-1}$; following Mann and Lazier (2005)]	Ice-ocean ecosystem model for 1-D and 3-D applications in the Bering and Chukchi seas.
Tedesco and Vichi (2010 and e.g. 2019)	None	Biogeochemical flux model in sea ice
Vancoppenolle et al. (2010)	Diffusion parameterized as a function of the Rayleigh number	Modelling brine and nutrient dynamics in Antarctic sea ice
Jeffery et al. (2011)	Diffusion parameterized as a function of the Rayleigh number	Los Alamos Sea Ice Model
Mortenson et al. (2017)	Diffusion parameterized as a function of friction velocity	Biogeochemical model representing the low trophic levels of sea ice and pelagic ecosystems in the Arctic.

93 2 Methods

94 2.1 Concepts

95 ~~Eq. (1) from Cota et al. (1987) provides the basis for our reasoning about nutrient exchanges between the ocean and the sea~~
96 ~~ice bottom being based on a turbulent exchange process enhanced by current velocity shear, irrespective of other exchanges~~
97 ~~based on brine dynamics, ice melt and ice growth. These turbulent exchanges may be parameterized through the flux of a~~
98 quantity at the interface between the ocean and the sea ice, calculated as the product of a scale velocity and the change in the
99 quantity from the boundary to some reference level (McPhee, 2008):

$$100 \langle w' S' \rangle = \alpha_s u^* (S_w - S_0) \quad (21)$$

101 Where, ~~$\langle w' S' \rangle$~~ represents the averaged co-variance of the turbulent fluctuations of ~~are~~ interface vertical velocity (m s^{-1})
102 and salinity, respectively, α_s is an interface salt/nutrient exchange coefficient (dimensionless); u^* is the friction velocity (m s^{-1});
103 S_0 and S_w are interface and far-field salinities, respectively.

104 Hereafter we will assume that salt turbulent exchanges are similar to nutrient exchanges and governed by the same principles
105 and parameters. The main difference between turbulent heat and salt/nutrient exchanges is due to the exchange coefficients
106 that may be higher for heat. The heat exchange coefficient (α_h) is around 0.006. The ratio (R) between α_h and α_s may vary from
107 unity to a range between 35 and 70 during ice melting and because of double diffusion, leading to a range in α_s between 8.6
108 10^{-5} and 0.006 (McPhee et al., 2008).

109 The net downward heat flux from the ice to the ocean in the Los Alamos Sea Ice Model (CICE + Icepack) is given by (Hunke
110 et al., 2015) and it is computed according to MCPhee et al. (2008) [Eq. (2)]:

$$111 F_{bot} = -\rho_w c_w \alpha_h u^* (T_w - T_f) \quad (32)$$

112 Where, ρ_w is the density of seawater (kg m^{-3}); c_w is the specific heat of seawater ($\text{J kg}^{-1} \text{ K}^{-1}$); α_h is the heat transfer coefficient
113 (dimensionless); T_w is the water temperature (K); T_f if the freezing temperature (K).

114 We calculate salt or nutrient exchanges using a similar approach:

$$F_N = -\alpha_s u^* (N_w - N_{i0}) \quad (43)$$

In fact, this ~~agrees is an extension of the concept used for heat and salt with by~~ McPhee (2008) (see page 112, Fig. 6.3). The minus sign used in (3) and (4) is for compatibility with the CICE + Icepack convention that upward fluxes are negative (e.g. Hunke et al., 2015).

A timescale for this turbulent process may be calculated from:

$$\tau = \frac{\alpha_s u^*}{kz} [s^{-1}] \quad (54)$$

Where ~~h is the a vertical distance over which diffusion is to be calculated~~ (m) (~~h in the Los Alamos Sea Ice Model, see below~~). ~~In the Los Alamos Sea Ice Model, it corresponds to the layer thickness of the biogeochemical grid (biogrid), used for discretizing the vertical transport equations of biogeochemical tracers and defined between the ice bottom and the brine height (Jeffery et al., 2016)~~. The above time scale is calculated for consistency with CICE implementation of diffusion, where a comparable time scale is calculated as:

$$\tau = \frac{D_m}{h^2} [s^{-1}] \quad (65)$$

Or

$$\tau = \frac{D_{MLD}}{h^2} [s^{-1}] \quad (76)$$

Where D_m is the molecular diffusion coefficient and D_{MLD} is the mixed length diffusion coefficient ($m^2 s^{-1}$) (Jeffery et al., 2011). ~~In the Los Alamos Sea Ice Model, h corresponds to the thickness of the biogeochemical grid (biogrid). This is the non-dimensional grid used for discretizing the vertical transport equations of biogeochemical tracers, defined between the brine height, which takes the value zero, and the ice-ocean interface, which takes the value one (Jeffery et al., 2016). The usage of h in these timescales implies merely the way they are normalized in the code before the actual diffusive fluxes are calculated considering the relative distance between the points ($h \cdot \partial x$, see below equation 7) where variables are calculated, along the layers of the biogrid. The product $h \cdot x$ corresponds to the actual distance of a given point from the top of the biogrid.~~ These time scales expressed in equations ~~6-5~~ and ~~7-6~~ are included in the Icepack transport equation, which may be written as [for more details, refer Jeffery et al. (2011; 2016)]:

$$\varphi \frac{\partial N}{\partial t} = \left\{ \frac{(x-1)}{h} \frac{\partial z_t}{\partial t} - \frac{x}{h} \frac{\partial z_b}{\partial t} \right\} \frac{\partial}{\partial x} (\varphi N) + \frac{1}{h} \frac{\partial}{\partial x} (w_f N) + \frac{\partial}{\partial x} \left(\frac{D_{MLD} + \varphi D_m}{h^2} \frac{\partial N}{\partial x} \right) \quad (87)$$

Where $0 \leq x \leq l$ is the relative depth of the vertical domain of the biogrid, z_t and z_b are vertical ~~distances-positions from the of interface between the ocean the sea ice the ice top and bottom~~ (m), ~~respectively~~. φ is sea ice porosity, w_f is the Darcy velocity due to the sea ice flushing of tracers ($m s^{-1}$). D_{MLD} is detailed in Jeffery et al. (2011) and it is zero when the brine vertical density gradient is stable, otherwise (when density increases towards the ice top) it is calculated as:

$$D_{MLD} = \frac{gk}{\mu} \Delta \rho_e l \quad (98)$$

Where g is the acceleration of gravity ($9.8 m s^{-2}$), k is sea ice permeability, μ is dynamic viscosity ($2.2 kg m^{-1} s^{-1}$), ρ_e is the equilibrium brine density and l is a length scale (7 m). The values shown here are the default ones in Icepack.

~~We rewrite the last term of 7-8 for the bottom ice layer as~~

147 [The last term of equation 7 includes the contribution of molecular diffusion that is calculated at the interface of all layers of](#)
148 [the biogrid and at the interface of the last layer and the ocean. In the simulations using turbulent diffusion, we perform the](#)
149 [same calculations, except that the molecular diffusion term \$\frac{\phi D_m}{h^2}\$ is replaced with a turbulent diffusion term \$\frac{\alpha_s u^*}{h}\$ at the interface](#)
150 [between the last model layer and the ocean.](#)

151

(10)

152 The transport equation is resolved along the biogrid, with a Flux-Corrected, Positive Definite Transport Scheme, using the
153 finite element Galerkin discretization (Jeffery et al., 2016). [In the case of the bottom ice layer, tracer concentrations are](#)
154 [calculated at the ice-ocean interface.](#)

155 Therefore, [in the CICE model](#) the implementation of turbulent diffusion nutrient exchanges [at the ice-ocean interface](#) in terms
156 consistent with ~~momentum and~~ heat exchanges is quite straightforward ~~in the CICE model~~, depending on changing the
157 timescales from Eq. (65) ~~or (7)~~ to (54). In other models, other approaches may be required.

158 From equations 5-4 - 7-6 it turns out that the product $\alpha_s u$ ~~by distance (z) *h~~ has the same dimensions of D_m or D_{MLD} ,
159 corresponding to a turbulent diffusion coefficient. Assuming $h_z \approx 0.01$ m, turbulent diffusion induced by velocity shear,
160 becomes comparable with molecular diffusion only for $u^* < 0.0012$ m s⁻¹, considering the lower end of the α_s range ($8.6 \cdot 10^{-5}$,
161 see above) or $u^* < 1.7 \cdot 10^{-5}$ m s⁻¹, considering the upper end of the α_s range (0.006). If we assume instead $h_z \approx 0.001$ m, the
162 calculated u^* values ~~become increase by~~ one order of magnitude ~~higher~~ but ~~are~~ still very low. In fact, such low friction
163 velocities would require extremely low “stream” velocities - relative ice-ocean velocities. For an account of the relationship
164 between “stream” and friction velocities under the sea ice see Supplementary information 3 of Olsen et al. (2019) and
165 references therein. These authors show that “stream” velocities of only a few centimetres per second lead to friction velocities
166 one order of magnitude lower but still in the order of 0.001 ms⁻¹, i.e., comparable only to the highest u^* estimated above.
167 Considering current velocities relative to the sea ice observed during the N-ICE2015 cruise [Granskog et al., 2018; Figure 2d
168 of Duarte et al. (2017)], with most values between 0.05 and > 0.2 m s⁻¹, it is rather likely that friction velocities under the ice
169 are frequently above the thresholds calculated above and that turbulent diffusion will dominate over molecular diffusion.
170 Dalman et al. (2019) provided experimental evidence for such turbulent nutrient fluxes to the ice bottom, leading to increased
171 chlorophyll concentrations at the bottom ice, in a strait with strong tidal currents. The mechanism treated here as turbulent
172 diffusion seems analogous to “forced convection” in the lowermost parts of the brine network, which is driven by pressure
173 differences caused by the shear under the sea ice (Neufeld, 2008; Vancoppenolle et al., 2013).

174 2.2 Implementation

175 We used the Los Alamos Sea Ice Model, which is managed by the CICE Consortium with an active forum
176 (<https://bb.cgd.ucar.edu/cesm/forums/cice-consortium.146/>) and a git repository (<https://github.com/CICE-Consortium>). It
177 includes two independent packages: CICE and Icepack. The former computes ice dynamic processes and the latter ice column
178 physics and biogeochemistry. Their development is handled independently with respect to the GitHub repositories

179 (https://github.com/CICE-Consortium). All the changes described below were implemented in two forks to the above
180 repository, one for Icepack and another for CICE and they may be found in Duarte (2021a and b, respectively).
181 Our simulations may be run using only Icepack, since they are focused on ice column physics and biogeochemistry, without
182 the need to consider ice dynamic processes. However, we used both CICE + Icepack together to allow for use of netCDF based
183 input/output not included in Icepack. Therefore, we defined a 1D vertically resolved model with 1 snow layer and 15 ice layers
184 and 5X5 horizontal cells. This is the minimum number of cells allowable in CICE due to the need to include halo cells (only
185 the central “column” is simulated). Therefore, ice column physics and biogeochemistry were calculated by Icepack but CICE
186 was the model driver. The input file (ice_in) used in this study was included in our CICE fork and it lists all parameters used
187 in the model and described in Hunke et al. (2016), Jeffery et al. (2016), Duarte et al. (2017) and in Tables S1 and S2. Any
188 changes in “default” parameters or any other model settings will be specified.

189 We made several modifications in CICE to allow using forcing time series collected during the Norwegian ~~Young-young Sea~~
190 ~~sea Ice-ice Expedition~~ (N-ICE2015) expedition (Granskog et al., 2018) and described in Duarte et al. (2017) (see Fig. 2 of the
191 cited authors). These modifications were meant to allow reading of forcing data at higher frequencies than possible with the
192 standard input subroutines in the CICE file ice_forcing.F90.

193 When the dynamical component of CICE is not used, u^* is set to a minimum value instead of being calculated as a function of
194 ice-ocean shear stress (Hunke et al., 2015). Duarte et al. (2017) implemented shear calculations from surface current velocities
195 (one of the models forcing functions) irrespective of ~~using or not~~ the use of the CICE dynamics code. These modifications were
196 also incorporated in the current model configuration so that shear can be used to calculate friction velocity and, thereafter,
197 influence heat and tracer/nutrient exchanges, following Eqs. (3) and (4) and parameters described in McPhee et al. (2008).
198 When the parameter k_{dyn} is set to zero in ice_in, ice dynamics is not computed, but shear is calculated in the modified
199 subroutine icepack_step_therm1, file icepack_therm_vertical.F90. If k_{dyn} is not zero, these calculations are ignored since
200 shear is already calculated in the dynamical part of the CICE code.

201 A Boolean parameter (Bottom_turb_mix) was added to the input file, which is set to “false” or “true” when the standard
202 molecular diffusion approach or the new turbulent based diffusion approach is ~~to be~~ used, respectively. Another Boolean
203 parameter (Limiting_factors_file) was added to the ice_in file. When set to “true” limiting factor values for light, temperature,
204 nitrogen, and silicate are written to a text file every model timestep. These are calculated by Icepack biogeochemistry,
205 according to Jeffery et al. (2016), but there is no writing-output option in the standard code.

206 **2.3 Model simulations**

207 Simulations were run for a refrozen lead (RL) without snow cover and for second-year sea ice (SYI) with ~40 cm snow cover
208 monitored in April-June during the N-ICE2015 expedition (Granskog et al., 2018 and Fig. 1 of Duarte et al. 2017). Details on
209 model forcing with atmospheric and oceanographic data collected during the N-ICE2015 expedition, including citations and
210 links to the publicly available datasets are given in Fig. 2 and section 3 of Duarte et al. (2017) and in the Supporting information
211 file. These data sets include wind speed, air temperature, precipitation, and specific humidity (Hudson et al., 2015); incident

212 surface short and longwave radiation (Hudson et al., 2016); ice temperature and salinity (Gerland et al., 2017); sea surface
213 current velocity, temperature, salinity and heat fluxes from a turbulence instrument cluster (TIC) (Peterson et al., 2016); sea
214 surface nutrient concentrations (Assmy et al., 2016) and sea ice biogeochemistry (Assmy et al., 2017). Ocean forcing is based
215 on measurements within the surface 2 meters which provide the boundary condition for the sea ice model. Model forcing files
216 may be found in Duarte (2021c).

217 Refrozen lead simulations started with zero ice, whereas Second Year Ice Simulations started with initial conditions described
218 in the Supporting information file (Table S3).

219 We ran simulations with the standard formulations for biogeochemical processes described in Jeffery et al. (2016) and settings
220 described in Duarte et al. (2017), using mushy thermodynamics, vertically resolved biogeochemistry, and including: freezing,
221 flushing, brine mixed length and molecular diffusion within the ice and at the interface between the ocean and the sea ice as
222 nutrient exchange mechanisms (Jeffery et al., 2011, 2016). We contrasted the above simulations against others that replaced
223 brine molecular and mixed length diffusion of nutrients at the interface between the ocean and the sea ice with diffusion driven
224 by current velocity shear (~~Table 2~~[Table 1](#)), calculated similar to heat ~~and momentum~~ exchanges, and following the
225 parameterization described in McPhee et al. (2008) and detailed above (equations 2 - ~~107~~). This contrast provides insight into
226 the effects of velocity shear on nutrient diffusion, ice algal production ($\text{mg C m}^{-2} \text{d}^{-1}$), chlorophyll standing stocks ($\text{mg Chl } a$
227 m^{-2}) and vertical distribution of chlorophyll concentration ($\text{mg Chl } a \text{ m}^{-3}$) [note that CICE model output for algal biomass in
228 mmol N m^{-3} was converted to $\text{mg Chl } a \text{ m}^{-3}$ as in Duarte et al. (2017), using $2.1 \text{ mg Chl } a \text{ mmol N}^{-1}$ and following Smith et al.
229 (1993)]. However, due to the concurrent effects of algal biomass exchange between the ocean and ice, such a contrast is not
230 enough to explicitly test our hypothesis and conclude about the effects of turbulent-driven nutrient supply on ice algal nutrient
231 limitation. Therefore, simulations were also run contrasting the same model setups, as described above, but restarting from
232 similar algal standing stocks and vertical distributions within the ice and, switching off algal inputs from the water to the ice.
233 This was done by nullifying the variable `algalN`, defining the ocean surface background ice algal concentration, in file
234 `icepack_zbgc.F90`, subroutine `icepack_init_ocean_bio` and in the restart files. In the case of the RL simulations that started
235 with zero ice, first a simulation was run until the 12 May, and then the obtained ice conditions were used to restart new
236 simulations without algal inputs from the ocean (`algalN = 0 mmol N m-3`). This way, when the simulations restarted, there was
237 already an ice algal standing stock necessary for the modelling experiments developed herein. The SYI simulations were, by
238 default, “restart simulations”, beginning with observed ice physical and biogeochemical variables. Therefore, there was already
239 an algal standing stock in the ice from the onset (Text S1 and Table S3).

240 McPhee et al. (2008) estimated different values for α_s , depending on whether the sea ice is growing (highest value) or melting
241 (lowest value) (~~Table 2~~[Table 1](#)). When running simulations for the RL, in some cases, we used only the minimum or the
242 maximum values for α_s , to allow for a more extreme contrast between molecular and turbulent diffusion parameterizations.
243 This was done since the former value will tend to minimize differences, whereas the latter will tend to emphasize them. We
244 also completed simulations for the RL and for SYI changing between the maximum and the minimum values of α_s , when ice
245 was growing or melting, respectively, and following McPhee et al. (2008) (see ~~Table 2~~[Table 1](#) for details). This

246 parameterization with a variable α , is likely the most realistic one, accounting for double diffusion during ice melting (McPhee
247 et al., 2008).

248 Apart from contrasting the way bottom-ice exchanges of nutrients were calculated, some simulations contrasted different
249 parameters related to silicate limitation (~~Table 2~~[Table 1](#)). This approach follows Duarte et al. (2017), where simulations were
250 tuned by changing the Si:N ratio and the half saturation constant for silicate uptake because silicate limitation was leading to
251 an underestimation of algal growth. From this exercise we were able to assess if such tuning was still necessary after
252 implementing turbulent diffusion at the interface between the ocean and the sea ice, driven by velocity shear. Moreover, we
253 repeated simulations with varying snow heights to further investigate the interplay between light and nutrient limitation under
254 contrasting nutrient diffusion parameterizations (~~Table 2~~[Table 1](#)).

255

256

257

258

259

260

261

262

263

264

265

266

267

268

269

270

271 Table 21. Model simulations. Refrozen lead (RL) simulation RL_Sim1 corresponds to RL_Sim5 described in Duarte et al. (2017) - the simulation leading
 272 to a best fit to the observations in that study. The remaining RL simulations 2 – 5 differ from RL_Sim1 in using turbulent diffusion at the interface between
 273 the ocean and the sea ice for nutrients in a comparable way as it is calculated for heat and driven by velocity shear. Moreover, RL_Sim5 differs in the
 274 concentration of ice algae in the water column that colonize the sea ice bottom (algalN) and in silicate limitation related parameters. These changes were
 275 done iteratively to fit the model to the observations. In RL_Sim2 and RL_Sim3 the maximum ($\alpha_s=0.006$) and the minimum ($\alpha_s=0.006/70=8.6 \cdot 10^{-5}$) values
 276 recommended by McPhee et al. (2008), respectively, are used throughout the simulations, to provide extreme case scenarios for comparison with RL_Sim1.
 277 In RL_Sim4, $\alpha_s=8.6 \cdot 10^{-5}$ when ice is not growing and 0.006 otherwise, as recommended by McPhee et al. (2008), to account for double diffusive processes
 278 during ice melting that slow down mass exchanges. The remaining RL simulations (RL_Sim6-9) are like the previous ones (RL_Sim1-4, respectively),
 279 except for algalN that was set to zero mmol N m⁻³, and all simulations were restarted with the same values for all variables. Therefore, simulations 6 – 9
 280 may differ only from 13 May 2015, when they were restarted. Second year ice simulation SYI_Sim_1 is based on Duarte et al. (2017) SYI_Sim4 but without
 281 algal motion. SYI_Sim2 and SYI_Sim3 use turbulent diffusion at the interface between the ocean and the sea ice. The former uses a decreased half
 282 saturation constant for silicate uptake, just like SYI_Sim1, whereas the latter uses the standard CICE value. The remaining SYI simulations (SYI_Sim4
 283 and 5) are like SYI_Sim1 and 2, except for algalN that was set to zero. Simulations SYI_Sim1 and SYI_Sim2 were repeated but with different initial snow
 284 thickness of 30, 20 and 15 cm to further investigate the interplay between light and silicate limitation (see text). Modified parameter values from one
 285 simulation to the next are marked in bold, separately for RL and SYI simulations. Modified parameters are based on literature ranges [e.g. Brzezinski
 286 (1985) and Hegseth (1992), for ratio_Si2N_diatoms, Nelson and Treguer (1992), for K_Sil_diatoms], Urrego-Blanco et al. (2016), for R_snw], or on
 287 previous model calibration work (Duarte et al., 2017). Parameters values were modified in the model input file ice_in, except for algalN and α_s , that are
 288 hard-coded.

Simulations	Modified parameters (bold types below indicate the parameter abbreviation used in Icepack)					
	Silica to nitrogen ratio in diatoms (ratio_Si2N_diatoms)	Half saturation constant for silicate uptake (K_Sil_diatoms, mM Si)	Ice algal concentration in the water (algalN, mM N)	Boolean to define the usage of either molecular (0) or turbulent diffusion (1) (<u>Bottom_turb_mi_xkdyb</u>)	Interface salt/nutrient turbulent exchange coefficient (α_s)	Sigma coefficient for snow grain (R_snw)
RL_Sim1	1.0	2.2	11 10 ⁻⁴	0	-	1.5
RL_Sim2	1.0	2.2	11 10 ⁻⁴	1	0.006	1.5
RL_Sim3	1.0	2.2	11 10 ⁻⁴	1	8.6 10⁻⁵	1.5
RL_Sim4	1.0	2.2	11 10 ⁻⁴	1	8.6 10⁻⁵-0.006	1.5
RL_Sim5	1.7	5.0	4 10⁻⁴	1	8.6 10 ⁻⁵ -0.006	1.5
RL_Sim6-9	As RL_Sim1-RL_Sim4, respectively		0	As RL_Sim1-RL_Sim4, respectively		
SYI_Sim1	1.0	2.2	11 10 ⁻⁴	0	-	0.8

SYI_Sim2	1.0	2.2	$11 \cdot 10^{-4}$	1	$8.6 \cdot 10^{-5} - 0.006$	0.8
SYI_Sim3	1.0	4.0	$11 \cdot 10^{-4}$	1	$8.6 \cdot 10^{-5} - 0.006$	0.8
SYI_Sim4 and 5	As SYI_Sim1 and SYI_Sim2, respectively		0	As SYI_Sim1 and SYI_Sim2, respectively		

289

291 3. Results

292 The results of the simulations listed in [Table 2Table 1](#) and presented below may be found in Duarte (2021d).

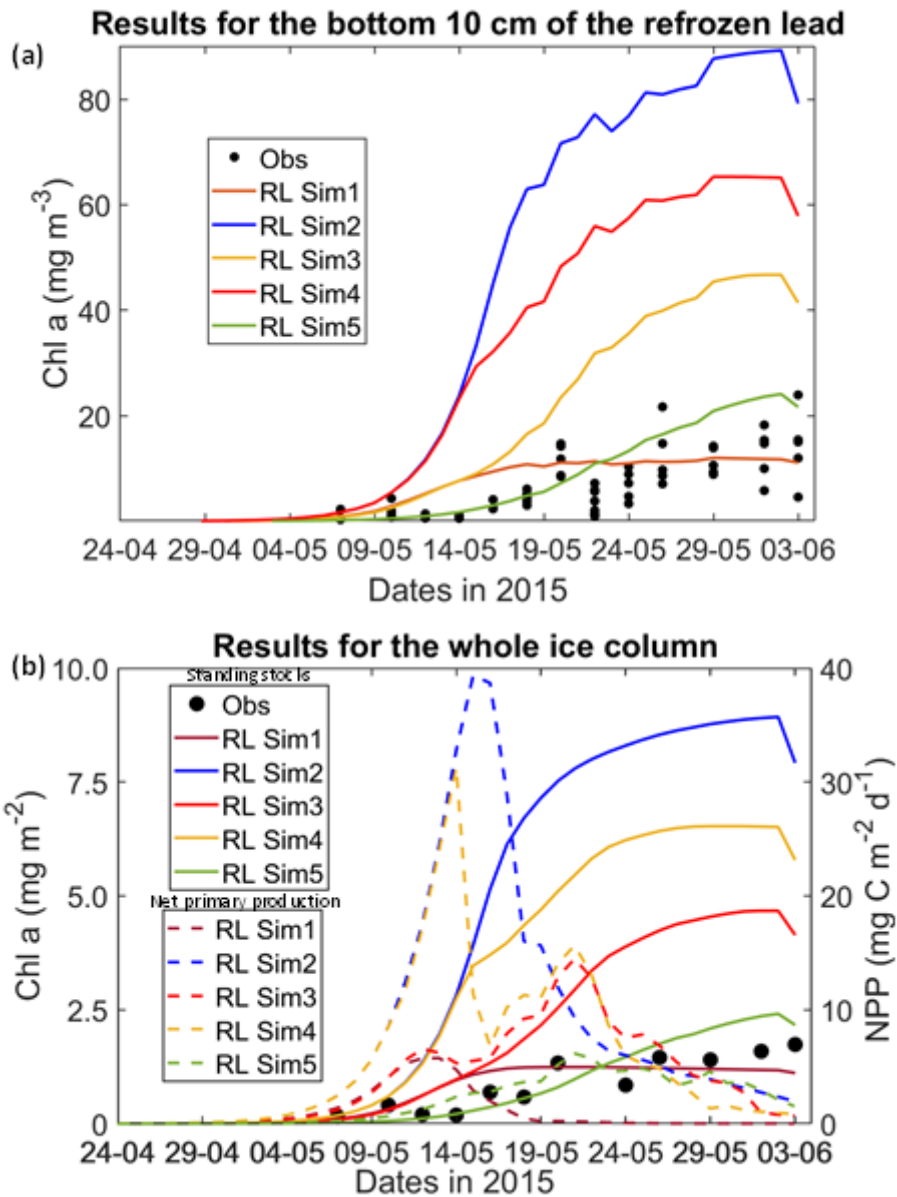
293 3.1 Refrozen lead simulations

294 All simulations with turbulent diffusion (RL_Sim2 – RL_Sim5, [Table 2Table 1](#)), predict higher bottom chlorophyll *a* (*Chl a*)
 295 concentration than with the standard molecular diffusion formulation (RL_Sim1) (Fig. 1a). Simulations RL_Sim2 - 4 grossly
 296 overestimate observations. Simulation RL_Sim3, using the lowest value for α_s , is closer both to observations and to RL_Sim1,
 297 as well as RL_Sim5, with the latter having the same α_s values of RL_Sim4 but a half saturation constant for silicate limitation
 298 increased from its tuned value in Duarte et al. (2017) of 2.2 μM to 5.0 μM and algalN reduced ([Table 2Table 1](#)) to bring model
 299 results closer to observations. Patterns between simulations for the whole ice column and considering both standing stocks and
 300 net primary production, are similar to those observed for the bottom-ice (Fig. 1b). Algal biomass is concentrated at the bottom
 301 layers (Fig. 2). Concentrations in the layers located between the bottom and the top of the biogrid, defined by the vertical
 302 extent (brine height) of the brine network (green lines in the map plots) (Jeffery et al., 2011) are $< 10 \text{ mg } Chl a \text{ m}^{-3}$. Ice
 303 thickness, temperature and salinity profiles are extremely similar among these simulations (Figs. S1 and S2).

304 Results for the silicate and nitrogen limiting factors are based on brine concentrations. Limiting factors exhibiting lower values
 305 (more limitation) in RL simulations are silicate, followed by light (Figs. 3, S3 – S5). Limiting values for silicate range between
 306 zero (maximum limitation) and one (no limitation), with stronger limitation after May 13 in all simulations (Fig. 3). The most
 307 severe silicate limitation is for RL_Sim1, where values drop to near zero around middle May. Despite the high average bottom
 308 *Chl a* concentration predicted in all simulations the bottom layer is where silicate limitation is less severe after May 13. This
 309 is more evident in simulations with turbulent bottom diffusion, where light limitation at the bottom-ice becomes more severe
 310 than silicate limitation around the end of May (Fig. S6).

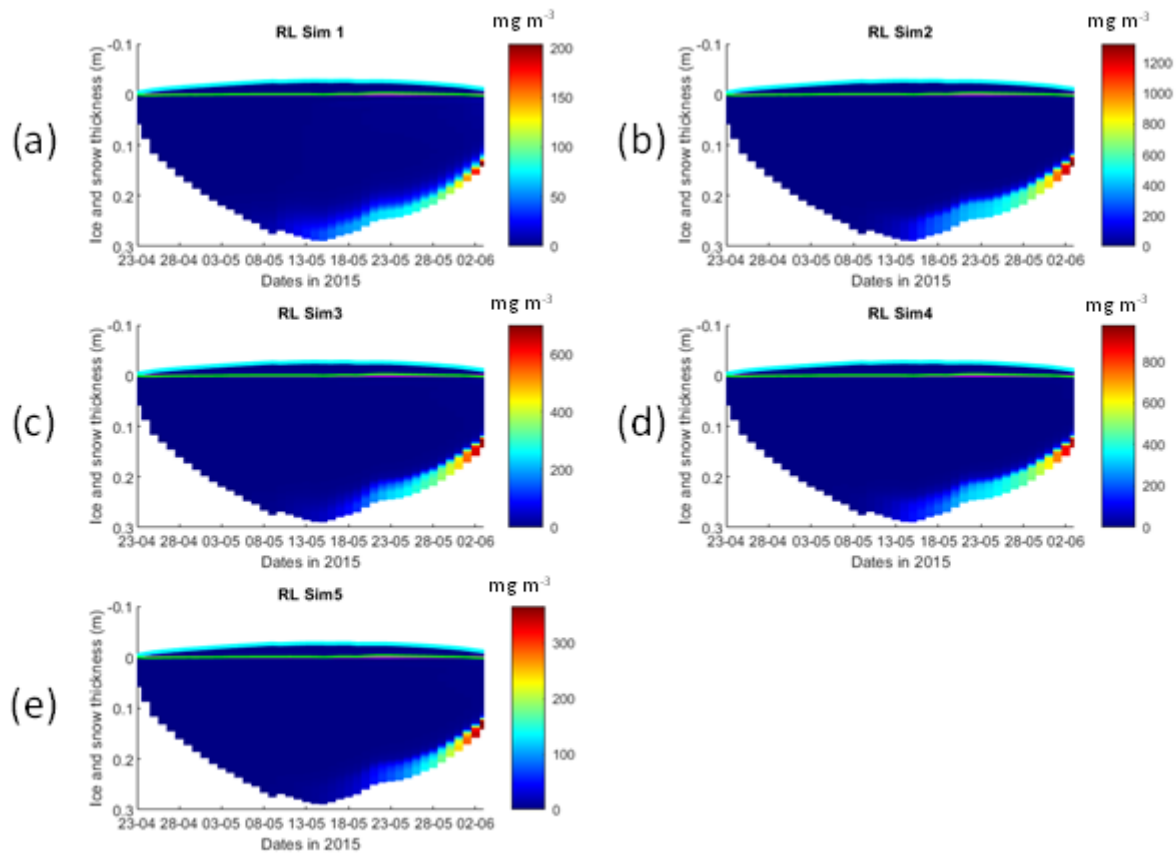
311 Results obtained with RL_Sim6-9, without algal exchanges between the ocean and the ice (see [Table 2Table 1](#)), show similar
 312 patterns of those observed with RL_Sim1-5, respectively (Fig. 4 versus Fig. 2, Fig. S9 versus Fig. 3, Figs. S7 and S8 versus
 313 Figs. S1 and S2, Figs. S10 – S12 versus Figs. S3 – S5).

314 Interface diffusivity (one of CICE diagnostic variables, corresponding to the diffusion coefficient between adjacent
 315 biogeochemical layers and between the bottom layers and the ocean) for simulations with turbulent exchanges ($\alpha_{s,u} * H$) are up
 316 to two orders of magnitude higher at the bottom (diffusivity between the bottom layer and the ocean) than for the RL_Sim1
 317 simulation with only molecular diffusion (D_m) ~~or D_m~~ + the mixed length diffusion coefficient (D_{MLD}) (refer 2.1 and Fig. 5).



319

320 **Figure 1. Daily averaged results for the refrozen lead (RL):** (a) Observed and modelled *Chl a* concentration values averaged for the
 321 ice bottom 10 cm; (b) Observed and modelled *Chl a* standing stock (continuous lines) and modelled net primary production (NPP)
 322 (dashed lines) for the whole ice column (refer to [Table 2](#)[Table 1](#) for details about model simulations). Observations are the same
 323 presented in Duarte et al. (2017).



324

325

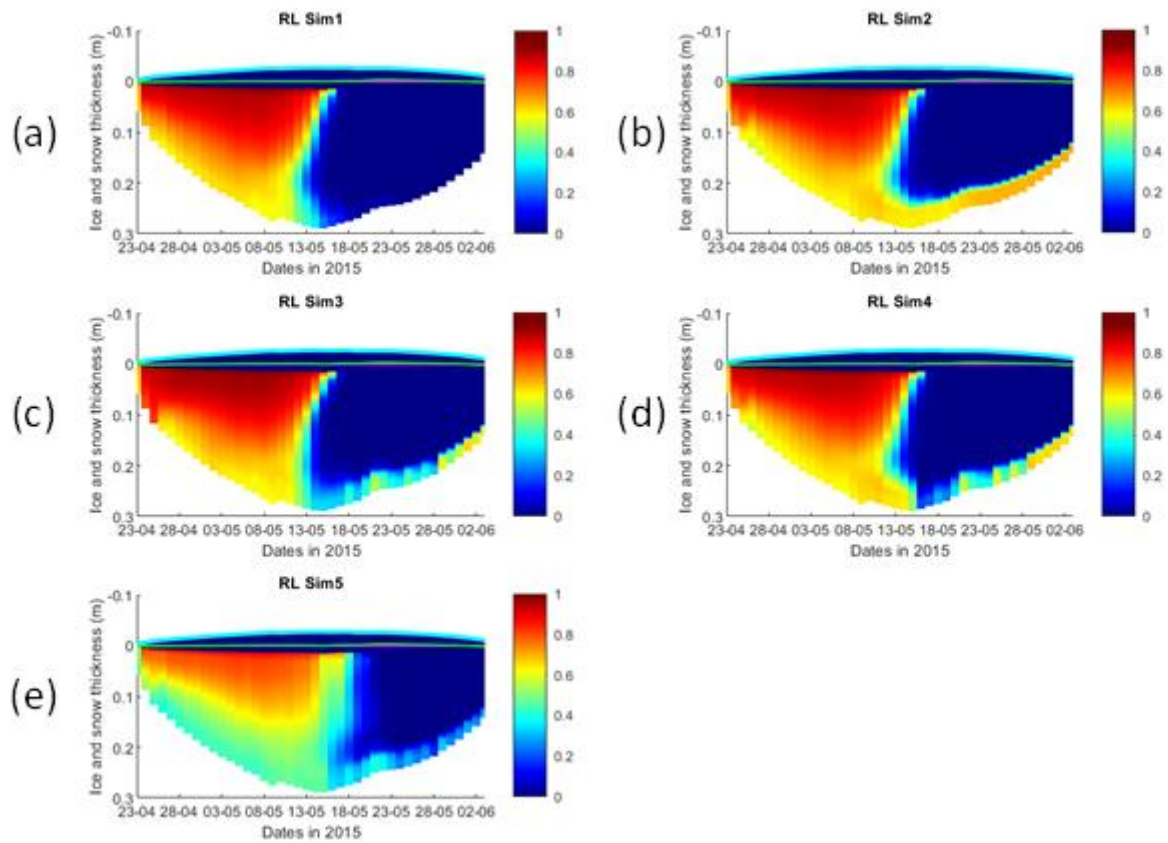
326

327

328

329

Figure 2. Daily averaged results for the refrozen lead (RL) simulations 1 - 5: Simulated evolution of ice algae *Chl a* as a function of time and depth in the ice (note the colour scale differences between the various panels). Ice thickness is given by the distance between the upper and the lower limits of the maps. The upper regions of the graphs, above the green line with zero values, are above the CICE biogrid and have no brine network. The magenta line, partly covered by the green line, represents sea level. Refer to [Table 2](#) for details about model simulations.



330

331

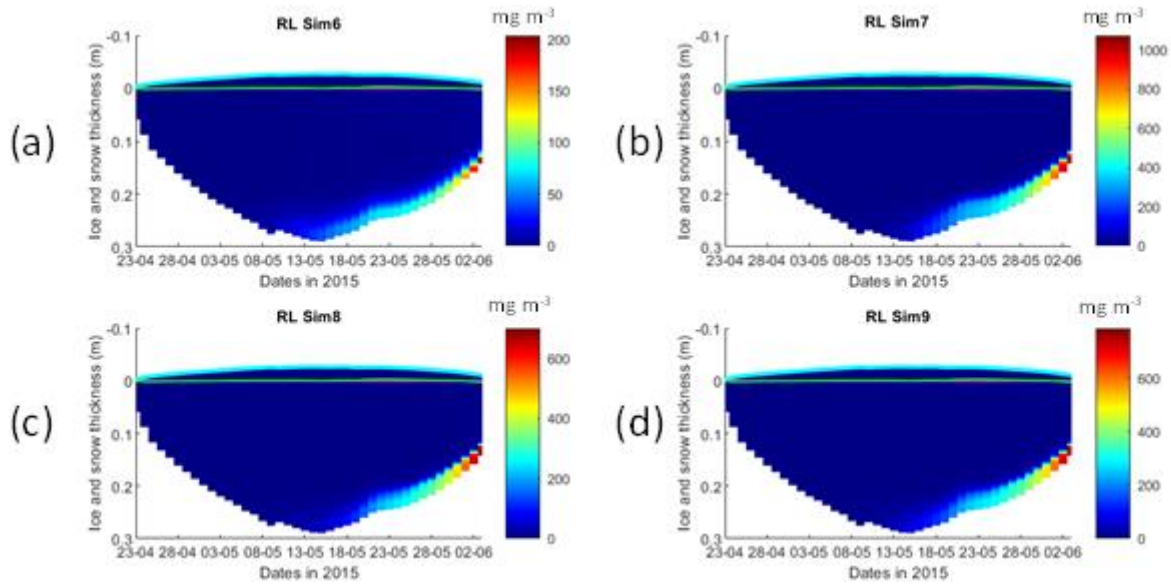
332

333

334

335

Figure 3. Daily averaged results for the refrozen lead (RL) simulations 1 - 5: Simulated evolution of silicate limitation (one means no limitation and zero is maximal limitation), as a function of time and depth in the ice. Ice thickness is given by the distance between the upper and the lower limits of the maps. The upper regions of the graphs, above the green line with zero values, are above the CICE biogrid and have no brine network. The magenta line, partly covered by the green line, represents sea level. Refer to [Table 2](#) for details about model simulations.



336

337

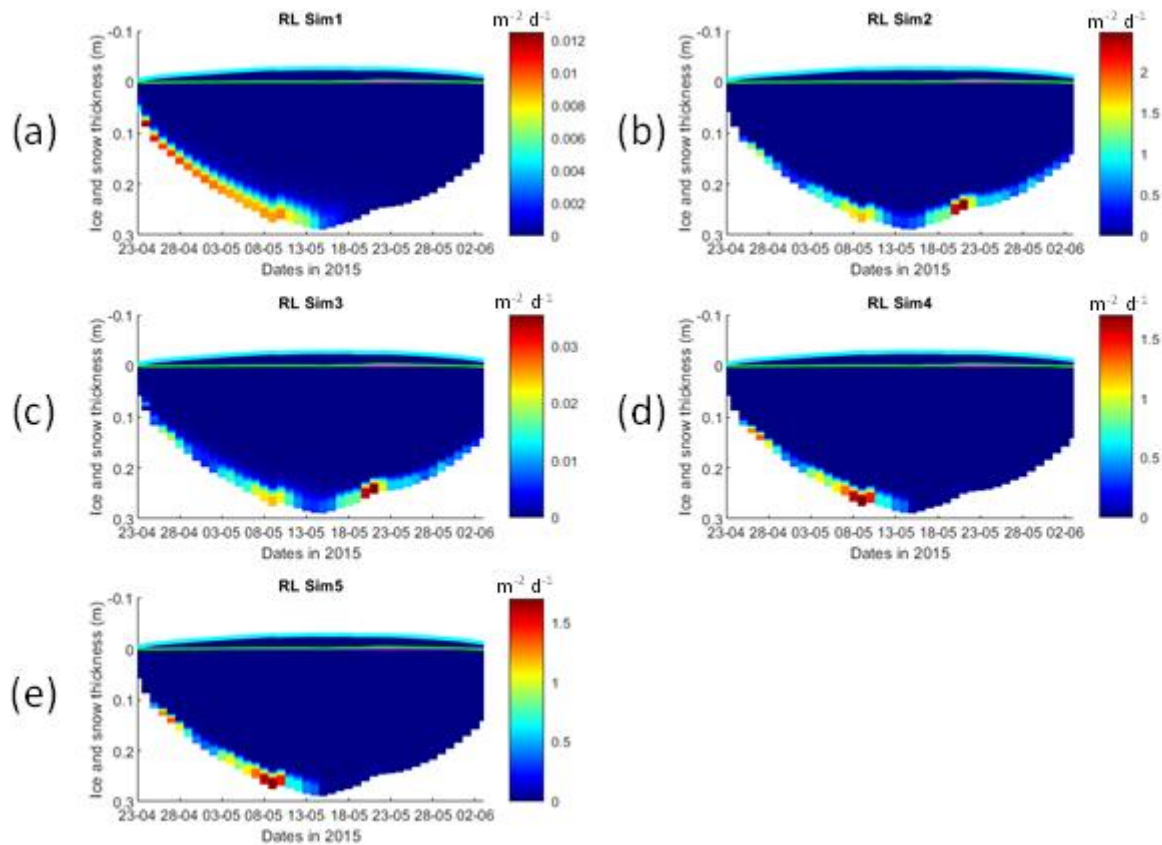
338

339

340

341

Figure 4. Daily averaged results for the refrozen lead (RL) simulations 6 - 9: Simulated evolution of ice algae *Chl a* as a function of time and depth in the ice (note the colour scale differences between the various panels). Ice thickness is given by the distance between the upper and the lower limits of the maps. The upper regions of the graphs, above the green line with zero values, are above the CICE biogrid and have no brine network. The magenta line, partly covered by the green line, represents sea level. Refer to [Table 2](#) [Table 1](#) for details about model simulations.



342

343 **Figure 5. Daily averaged results for the refrozen lead (RL) simulations 1-5: Simulated evolution of interface diffusivity as a function**
 344 **of time and depth in the ice (note the colour scale differences between the various panels). Ice thickness is given by the distance**
 345 **between the upper and the lower limits of the maps. The upper regions of the graphs, above the green line with zero values, are**
 346 **above the CICE biogrid and have no brine network. The magenta line represents sea level. Refer to [Table 2 Table 1](#) for details about**
 347 **model simulations.**

348

349 3.2 Second year ice simulations

350 Simulations with turbulent diffusion (SYI_Sim2 and 3), predict only slightly higher standing stocks and net primary production
 351 than with the standard molecular diffusion formulation (SYI_Sim1) (Fig. 6). The visual fit to the standing stock observations
 352 is comparable between the various simulations. Changing the half saturation constant for silicate limitation from 2.2 to 4.0 μM
 353 has no impact on model results. This is confirmed by analysing the evolution of *Chl a* concentration as a function of time and
 354 depth in the ice (Fig. 7), with only minor differences being apparent towards the end of the simulation, when *Chl a* increases

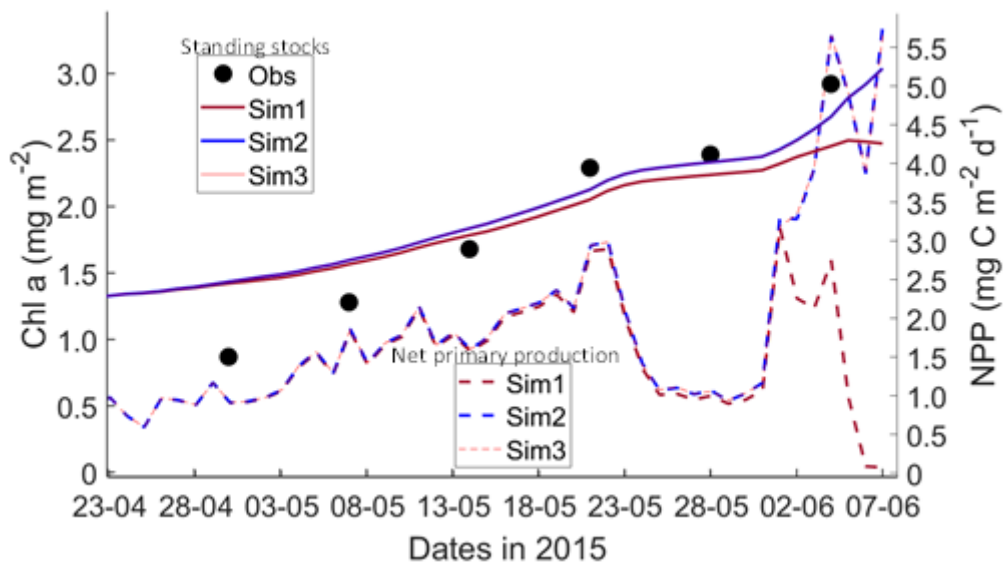
355 at the bottom layers in the simulations with turbulent diffusion (SYI_Sim 2 and 3). Ice thickness, temperature and salinity
356 profiles are extremely similar among these simulations (Fig. S13).

357 The dominant limiting factor in these simulations is light, followed by silicate (compare Fig. 8a, c and e with 8b, d and f and
358 with Fig. S14). Light limitation is less severe after the onset of snow and ice melting at the beginning of June. Silicate limitation
359 is very strong above the bottom ice. Nitrogen limitation is highest at a depth range between ~0.4 ~0.7 m below the ice top,
360 with a large overlap with the depth range where a *Chl a* maximum is observed (Fig. 7). Maximal *Chl a* concentration predicted
361 for the RL_Sim1 and RL_Sim5 simulations - those closer to observations - are two orders of magnitude higher than those
362 predicted for SYI (Fig. 2a and e versus Fig. 7). However, standing stocks predicted for RL_Sim1 and RL_Sim5 simulations
363 are smaller than for SYI simulations, as confirmed by the observations (Figs. 1b and 6). Opposite to what was described for
364 the RL simulations, silicate limitation becomes more severe than light limitation at the bottom layer only in SYI_Sim_1, at the
365 beginning of June, close to the end of the simulation (Fig. S15).

366 Results obtained without algal exchanges between the ocean and the ice (SYI_Sim4 and 5, see [Table 2Table 1](#)), show the same
367 patterns of those observed with SYI_Sim1 and 2, respectively (Fig. 9 versus Fig. 7, Fig. S17 versus Fig. 8, Figs. S18 versus
368 S14a - d and Figs. S16 versus S13a - d).

369 Interface diffusivity (one of CICE diagnostic variables, see above) for simulations with turbulent bottom exchanges are up to
370 four orders of magnitude higher at the bottom ice than for simulations with only molecular diffusion (Fig. S19, showing a
371 comparison between SYI_Sim1 and SYI_Sim2).

372 SYI_Sim1 and 2 were repeated with varying snow thickness ([Table 2Table 1](#) and Figs. 10 and 11). In the former simulation
373 (Fig. 10a), as snow height decreases, there is a reduction in light limitation and a sharp increase in silicate limitation, overtaking
374 light limitation (values becoming lower) as early as mid-May. In the latter simulation (Fig. 10b), light limitation prevails
375 irrespective of snow height, except in the case of the lower snow height of 15 cm where silicate becomes more limiting towards
376 the end of the simulation. With the decrease in snow height, there is an increase in *Chl a* concentration in all simulations.
377 Highest values for SYI_Sim2 are ~one order of magnitude larger than those for SYI_Sim1. Moreover, the decrease in snow
378 heights is followed by an earlier and more intense bottom ice algal bloom.



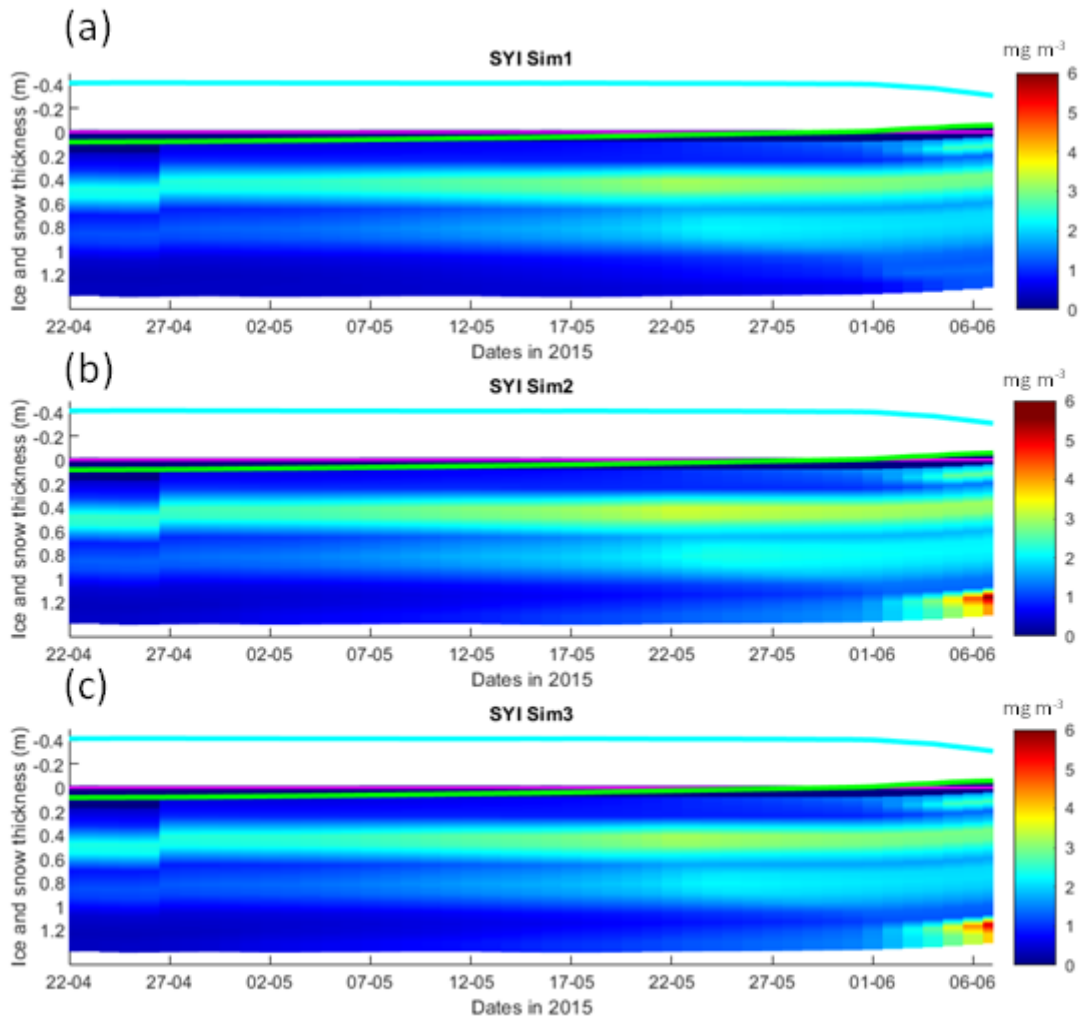
379

380

381

382

Figure 6. Daily averaged results for second year ice (SYI) simulations 1 - 3: Observed [same data presented in Duarte et al. (2017)] and modelled *Chl a* standing stock (continuous lines) and modelled net primary production (NPP) (dashed lines) for the whole ice column (refer to [Table 2](#)[Table 1](#) for details about model simulations).



383

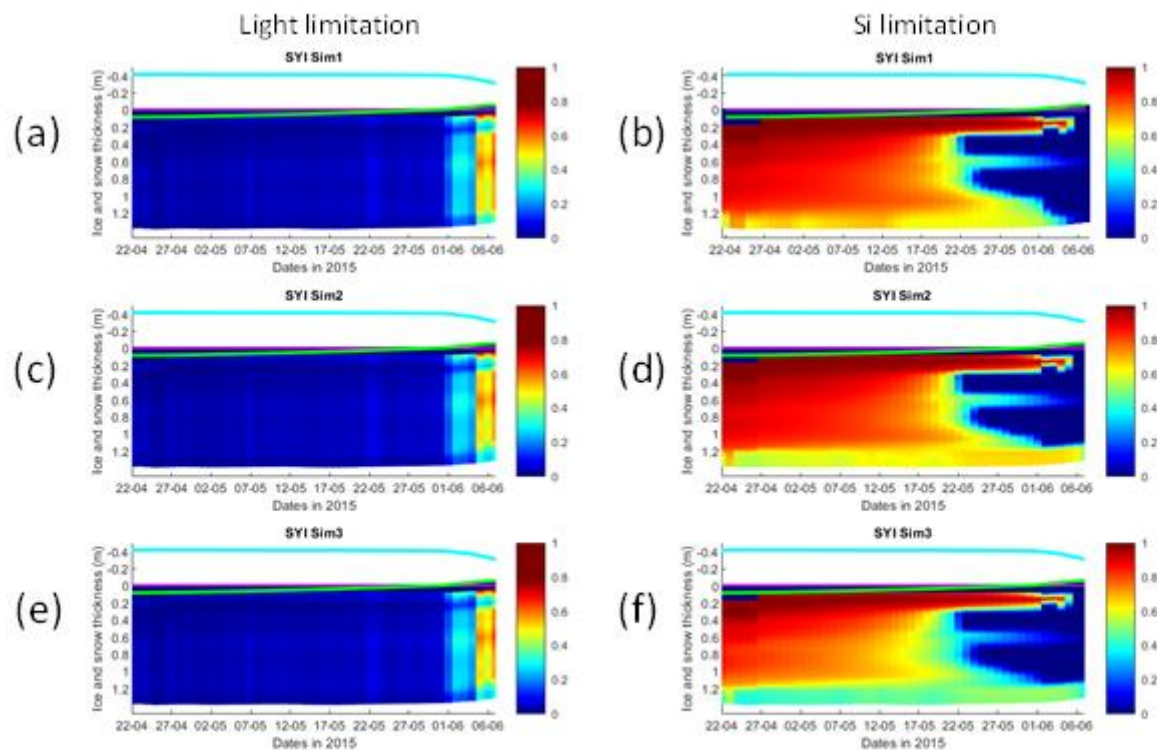
384

385

386

387

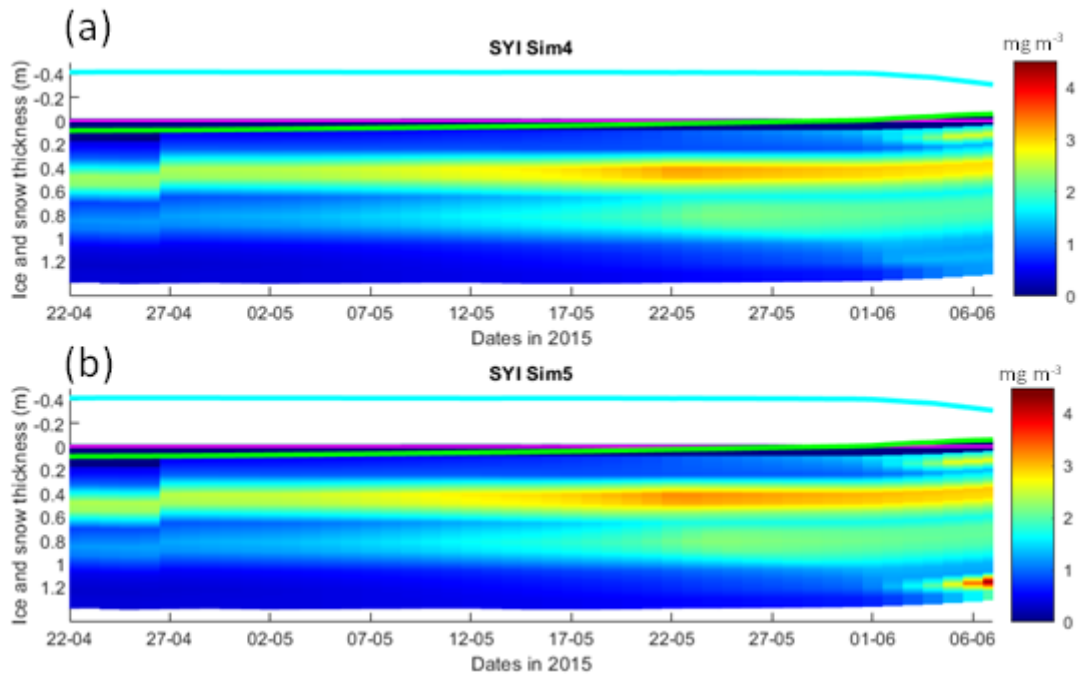
Figure 7. Daily averaged results for second year ice (SYI) simulations 1 - 3: Simulated evolution of ice algae *Chl a* as a function of time and depth in the ice. The upper regions of the graphs, above the green line with zero values, are above the CICE biogrid and have no brine network. The magenta line represents sea level, and the cyan line represents the top of the snow layer. Refer to [Table 2](#) for details about model simulations.



388

389

390 **Figure 8. Daily averaged results for second year ice (SYI) simulations 1 - 3: Simulated evolution of light (left panels) and silicate**
 391 **(right panels) limitation (one means no limitation and zero is maximal limitation), as a function of time and depth in the ice. The**
 392 **upper regions of the graphs, above the green line with zero values, are above the CICE biogrid and have no brine network. The**
 393 **magenta line represents sea level, and the cyan line represents the top of the snow layer. Refer to [Table 2](#) [Table 1](#) for details about**
model simulations.



394

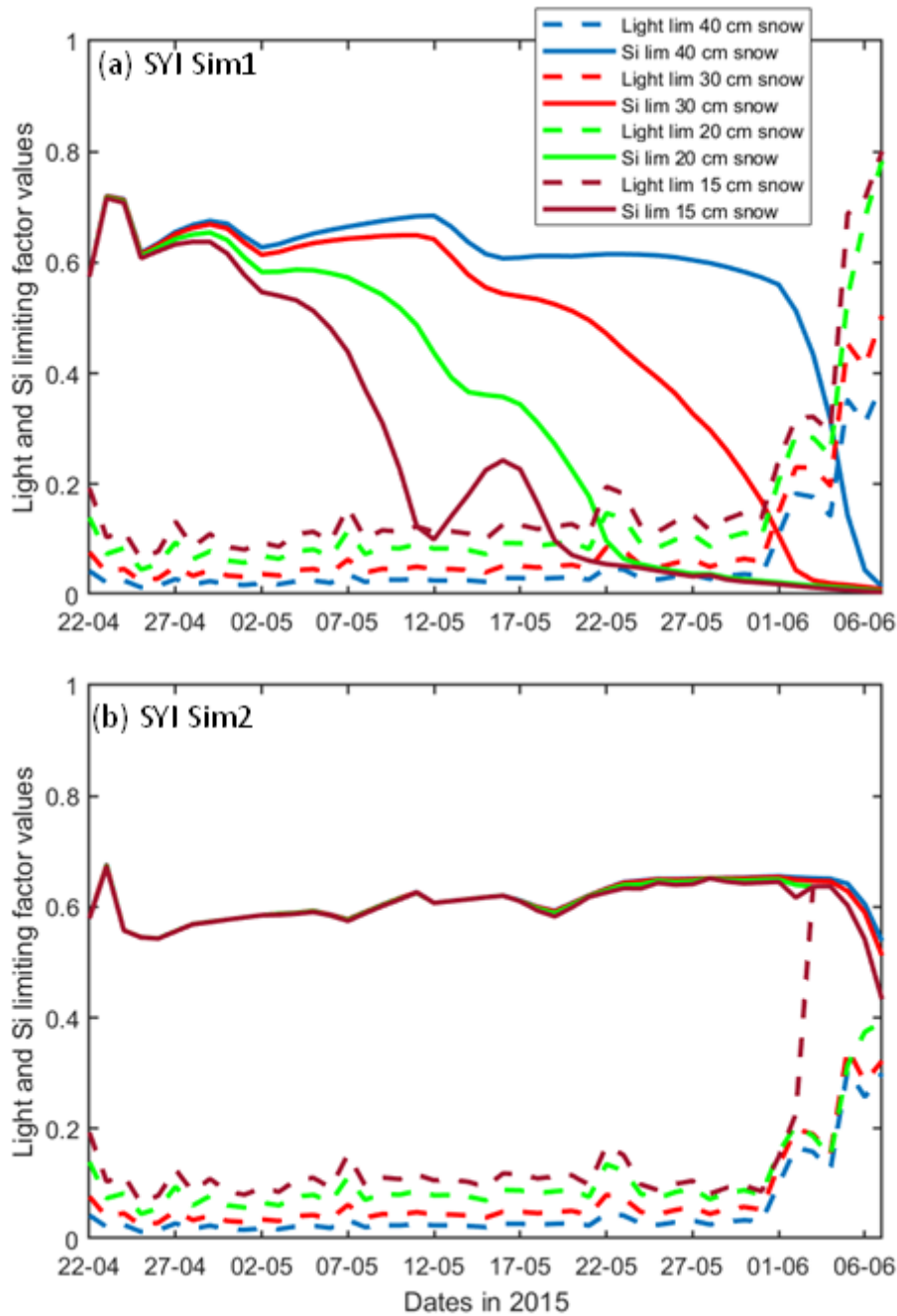
395

396

397

398

Figure 9. Daily averaged results for second year ice (SYI) simulations 4 and 5: Simulated evolution of ice algae *Chl a* as a function of time and depth in the ice. The upper regions of the graphs, above the green line with zero values, are above the CICE biogrid and have no brine network. The magenta line represents sea level, and the cyan line represents the top of the snow layer. Refer to [Table 1](#) for details about model simulations.



399

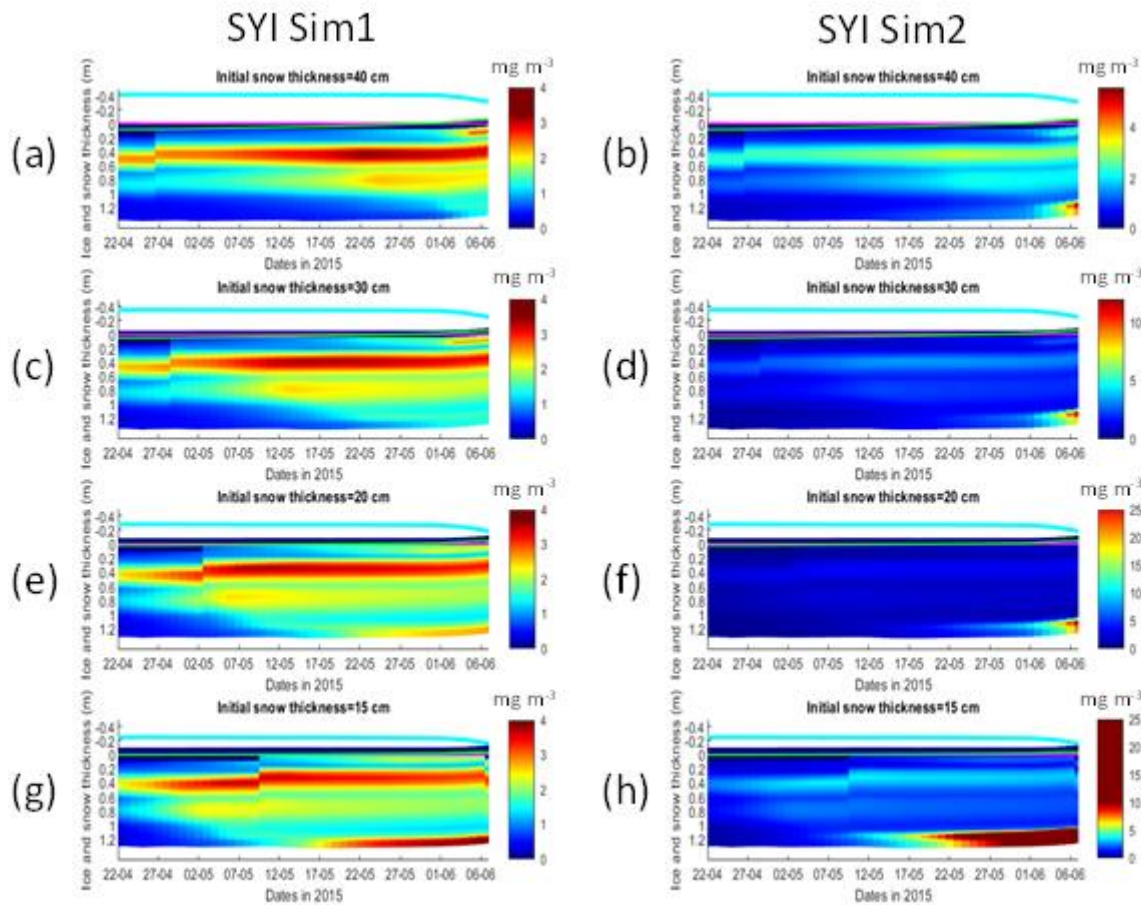
400

401

402

403

Figure 10. Daily averaged results for the second-year ice (SYI) simulations 1 (a) and 2 (b) starting with a snow depth of 40 (default simulation), 30, 20 and 15 cm: Simulated evolution of light (dashed lines) and silicate (continuous lines) limitation (one means no limitation and zero is maximal limitation), as a function of time at the ice bottom layer (one means no limitation). Refer to [Table 2](#) for details about model simulations.



404

405

406

407

408

409

Figure 11. Daily averaged results for second year ice (SYI) simulations 1 (left panels) and 2 (right panels) starting with a snow depth of 40 (default simulation), 30, 20 and 15 cm: Simulated evolution of ice algae *Chl a* as a function of time and depth in the ice. The upper regions of the graphs, above the green line with zero values, are above the CICE biogrid and have no brine network. The magenta line represents sea level, and the cyan line represents the top of the snow layer. Refer to [Table 2](#)/[Table 1](#) for a description of model simulations.

410

4. Discussion

411

412

413

414

415

416

The results obtained in this study support the initial hypothesis, showing that considering the role of velocity shear on turbulent nutrient exchanges between the ocean and the sea ice, formulated in a way consistent with ~~momentum and~~ heat exchanges, leads to a reduction in nutrient limitation that supports a significant increase in ice algal net primary production and *Chl a* biomass accumulation in the bottom ice layers, when production is ~~understood to be~~ nutrient limited. Therefore, our results are in line with empirical evidence provided by Cota et al. (1987) and Dalman et al. (2019) but, to the best of our knowledge, experimental evidence from properly ~~dedicated-designed~~ experiments is still lacking to test our hypothesis. Moreover, our

417 results do not imply necessarily that experiments carried out with other sea-ice models would render the same trends. The
418 implementation of turbulent mixing considerably relieved silicate limitation in the RL simulations, leading to an increase in
419 NPP, in the duration of the algal growth period, in bottom *Chl a* concentration and in-ice light absorption, increasing light
420 limitation due to shelf-shading [in the CICE model, optical ice properties are influenced by ice algal concentrations (Jeffery et
421 al., 2016)].

422 In the N-ICE2015 biogeochemical dataset (Assmy et al., 2016), the median of dissolved inorganic nitrogen to silicate ratios in
423 all surface and subsurface water masses, is above 1.7 (unpublished data), which is the upper limit for the nitrogen to silicate
424 ratio for polar diatoms (e.g. Takeda, 1998; Krause et al. 2018). Therefore, it can be expected that, in the region covered by the
425 N-ICE2015 expedition, silicate is more limiting than nitrogen for the production yields of the pennate diatoms characteristic
426 of the bottom-ice communities [the dominant algal functional group in bottom ice, e.g. Leu et al. (2015), van Leeuwe et al.
427 (2019)]. Elsewhere in the Arctic the opposite may be true, considering nitrate and silicate concentrations presented in Leu et
428 al. (2015) and the number of process studies documenting such limitation [e.g., Campbell et al. (2016)]. However, the
429 conclusions taken here about the effects of turbulent mixing are independent of the limiting nutrient.

430 Implementing turbulent diffusion between the ice and the ocean has obvious implications for model tuning. Our results for the
431 RL show that with this formulation it was necessary to increase the half saturation constant for silicate uptake and to reduce
432 the ocean concentration of algal nitrogen (algalN), reducing the colonization of bottom ice by ice algae, to obtain *Chl a* values
433 comparable to those observed (RL_Sim5). Therefore, whereas Duarte et al. (2017) had to reduce silicate limitation to improve
434 the fit between modelled and observational data, the opposite approach was required when using turbulent diffusion in line
435 with results reported in Lim et al. (2019) for Antarctic sea ice diatoms. This is an example of how one can get good model
436 results by the wrong reasons with difficult to predict consequences on model forecasts under various scenarios.

437 In the SYI case, only a minor increase in bottom *Chl a* concentration was observed towards the end of simulations SYI_Sim_2
438 and SYI_Sim_3, when light limitation due to the thick snow cover was relieved by snow melt. Silicate limitation was not as
439 severe as in SYI_Sim_1, due to greater bottom exchanges in the former simulations. The importance of snow cover in
440 controlling ice algal phenology has been stressed before [e.g., Campbell et al. (2015), Leu et al. (2015)].

441 Duarte et al. (2017) used the delta-Eddington parameter, corresponding to the standard deviation of the snow grain size
442 (R_{snow}) (Urrego-Blanco et al., 2016), to tune model predicted shortwave radiation at the ice bottom. However, there was
443 still a positive shortwave model bias in June. Therefore, our conclusion about the main limiting role of light in SYI is
444 conservative. Moreover, in part of SYI cores sampled during the N-ICE2015 expedition, in the period covered by our
445 simulations, with an unusually high snow thickness (~40 cm), there was no *Chl a* bottom maximum (Duarte et al., 2017; Olsen
446 et al., 2017).

447 The dominant role of light limitation in SYI was confirmed in the simulations with reduced snow thickness and alleviated light
448 limitation, with a bottom-ice algal *Chl a* maximum emerging earlier at snow thickness ≤ 20 cm. The reduction of snow heights
449 thickness had a much larger effect in increasing *Chl a* concentration at the bottom layer when turbulent mixing was used, due
450 to lower silicate limitation. Reducing snow height-thickness led to a relatively early shift from light to silicate limitation when

451 we used molecular and mixed length diffusion, whereas this shift occurred only at the very end of the simulated period when
452 we used turbulent diffusion at the ice-ocean interface, driven by velocity shear, instead of molecular diffusion. The effects of
453 different types of diffusion, upon reduction of the snow cover and the possible development of a bottom ice algal bloom, are
454 critical aspects when simulating ice algal phenology and attempting to quantify the contribution of sympagic-sea ice algae to
455 Arctic primary production.

456 Simulated shear-driven turbulent diffusivities are up to four orders of magnitude higher than molecular + mixed length
457 diffusivities at the bottom ice and the results presented herein emphasize their potential role in sea ice biogeochemistry. The
458 number and intensity of Arctic winter storms has increased over the 1979–2016 period (Rinke et al., 2017; Graham et al.,
459 2017) and the effect of more frequent and more intensive winter storms in the Atlantic Sector of the Arctic Ocean is a thinner,
460 weaker, and younger snow-laden ice pack (Graham et al., 2019). Storms that occur late in the winter season, after a deep
461 snowpack has accumulated, have the potential to promote ice growth by dynamically opening leads where new ice growth can
462 take place. The young ice of the refrozen leads does not have time to accumulate a deep snow layer until the melting season,
463 which could lead to light limitation of algal growth. All things considered, it can be expected that ongoing trends in the Arctic
464 will lead to a release from light limitation in increasingly larger areas of the ice pack in late winter, which will lead to more
465 likely nutrient limitation earlier in spring (e.g. Lannuzel et al. 2020). These effects will be further amplified under thinning of
466 the snowpack as observed in western Arctic, and in the Beaufort and Chukchi seas, over the last decades (Webster et al., 2014).
467 Therefore, properly parameterizing nutrient exchanges between the ice and the ocean in sea-ice biogeochemical models is of
468 utmost importance to avoid overestimating nutrient limitation and thus underestimating sea ice algal primary production.

469 In existing sea-ice models there are “natural” differences between the way budgets for non-conservative tracers such as
470 nutrients are closed compared to those of ~~momentum~~, heat and salt, which are related to the biogeochemical sinks and sources
471 (e.g., equation 18 in Vancoppenolle et al., 2010), but also some “inconsistencies”, related with the way their transfers between
472 the ocean and the ice are computed. Interestingly, some models (e.g., Jin et al., 2006, 2008 and Hunke et al., 2016) apply the
473 diffusion equation to calculate exchanges across the bottom ice not only to dissolved tracers, but also to algal cells. This is to
474 guarantee a mechanism of ice colonization by microalgae. However, the usage of the same coefficient for dissolved and
475 particulate components creates significant uncertainty.

476 Molecular diffusion is a slow process compared with ~~momentum and heat~~ turbulent exchanges. This justifies the usage of
477 diffusion coefficients which are much higher than molecular diffusivity, as in Jin et al. (2006), using a value of $1.0 \cdot 10^{-5} \text{ m}^2 \text{ s}^{-1}$,
478 four orders of magnitude higher than the value indicated in Mann and Lazier (2005) – $1.5 \cdot 10^{-9} \text{ m}^2 \text{ s}^{-1}$ – or the parameterization
479 of diffusivity as a function of friction velocity as in Mortenson et al. (2017). The approach proposed herein, formulating
480 bottom-ice nutrient exchanges in a way that is consistent with ~~momentum and~~ heat exchanges, provides a physically sound,
481 consistent, and easy to implement alternative.

482 **5. Conclusions**

483 Considering the role of velocity shear on turbulent nutrient exchanges at the interface between the ocean and the ice in a sea-
484 ice biogeochemical sub-model, leads to a reduction in nutrient limitation and a significant increase in ice algal net primary
485 production and *Chl a* biomass accumulation in the bottom-ice layers, when production is nutrient limited. The results presented
486 herein emphasize the potential role of bottom-ice nutrient exchange processes, irrespective of brine dynamics and other
487 physical-chemical processes, in delivering nutrients to bottom-ice algal communities, and thus the importance of properly
488 including them in sea-ice models. The relevance of this becomes even more apparent considering ongoing changes in the
489 Arctic icescape, with a predictable decrease in light limitation as ice becomes thinner and more fractured, with an expected
490 reduction in snow cover.

491 **Code availability**

492 The software code used in this study may be found at:

493 <https://doi.org/10.5281/zenodo.4675097> and <https://doi.org/10.5281/zenodo.4675021>

494 This code is in a fork derived from the CICE Consortium repository (<https://github.com/CICE-Consortium>).

495 The Consortium's codes are open-source with a standard 3-clause BSD license and are is under the following Copyright
496 license, available at (<https://cice-consortium-cice.readthedocs.io/en/master/intro/copyright.html>):

497

498 **Data availability**

499 Model forcing function files may be found at: <https://doi.org/10.5281/zenodo.4672176>

500 Results from model simulations described above, in the form of CICE daily netCDF history files iceh.* may be found at:
501 <http://doi.org/10.5281/zenodo.4672210>

502 There is one directory for each simulation, and it includes besides the historical files the input file (ice_in) with the simulation
503 parameters.

504

505 **Authors contribution**

506 Pedro Duarte made the software changes, designed the experiments, performed the simulations and prepared the manuscript
507 with contributions from all co-authors.

508 Philipp Assmy contributed to the writing of the manuscript.

509 Karley Campbell contributed to the writing of the manuscript.

510 Arild Sundfjord contributed to the writing of the manuscript and to funding acquisition.

511

512 **Competing interests**

513 The authors declare that they have no conflict of interest.

514 **Acknowledgements**

515 This work has been supported by the Fram Centre Arctic Ocean flagship project “Mesoscale physical and biogeochemical
516 modelling of the ocean and sea-ice in the Arctic Ocean” (project reference 66200), the Norwegian Metacenter for
517 Computational Science application “NN9300K - Ecosystem modelling of the Arctic Ocean around Svalbard”, the Norwegian
518 “Nansen Legacy” project (no. 276730) and the European Union’s Horizon 2020 research and innovation programme under
519 grant agreement No 869154 ([project FACE-IT](#)). Contributions by K Campbell are supported by the Diatom ARCTIC project
520 (NE/R012849/1;03F0810A), part of the Changing Arctic Ocean program, jointly funded by the UKRI Natural Environment
521 Research Council and the German Federal Ministry of Education and Research (BMBF).

522 **References**

- 523 Arrigo, K. R., Kremer, J. N., and Sullivan, C. W.: A Simulated Antarctic Fast Ice Ecosystem, *J. Geophys. Res.*, 98, 17, 1993.
- 524 Assmy, P., Duarte, P., Dujardin, J., Fernández-Méndez, M., Fransson, A., Hodgson, R., Kauko, H., Kristiansen, S., Mundy, C.
525 J., Olsen, L. M., Peeken, I., Sandbu, M., Wallenschus, J., Wold, A.: N-ICE2015 water column biogeochemistry [Data set],
526 Norwegian Polar Institute, <https://doi.org/10.21334/npolar.2016.3ebb7f64>, 2017.
- 527 Assmy, P., Dodd, P. A., Duarte, P., Dujardin, J., Elliott, A., Fernández-Méndez, M., Fransson, A., Granskog, M. A., Hendry,
528 K., Hodgson, R., Kauko, H., Kristiansen, S., Leng, M. J., Meyer, A., Mundy, C. J., Olsen, L. M., Peeken, I., Sandbu, M.,
529 Wallenschus, J., Wold, A.: N-ICE2015 sea ice biogeochemistry [Data set], Norwegian Polar Institute,
530 <https://doi.org/10.21334/npolar.2017.d3e93b31>, 2017.
- 531 Brzezinski, M. A.: The Si-C-N Ratio of Marine Diatoms - Interspecific Variability and the Effect of Some Environmental
532 Variables, *J. Phycol.*, 21, 347-357, 1985.
- 533 Campbell, K., Mundy, C. J., Barber, D. G. and Gosselin, M.: Characterizing the sea ice algae chlorophyll a–snow depth
534 relationship over Arctic spring melt using transmitted irradiance, *J. Mar. Sys.*, 147, 76-84, doi:
535 <https://doi.org/10.1016/j.jmarsys.2014.01.008>, 2015.
- 536 Campbell, K., Mundy, C. J., Landy, J. C., Delaforge, A., Michel, C. and Rysgaard, S.: Community dynamics of bottom-ice
537 algae in Dease Strait of the Canadian Arctic. *Prog. Oceanogr.*, 149, 27-39, doi: <http://dx.doi.org/10.1016/j.pocean.2016.10.005>,
538 2016.
- 539 Carmack, E.: Circulation and Mixing in Ice-Covered Waters, in: *The Geophysics of Sea Ice. NATO ASI Series (Series B:
540 Physics)*, edited by Untersteiner N. Springer, Boston, MA. 641-712, https://doi.org/10.1007/978-1-4899-5352-0_11, 1986.
- 541 Cota, G. F., Prinsenberg, S. J., Bennett, E. B., Loder, J. W., Lewis, M. R., Anning, J. L., Watson, N. H. F., and Harris, L. R.:
542 Nutrient Fluxes during Extended Blooms of Arctic Ice Algae, *J. Geophys. Res.-Oceans*, 92, 1951-1962, doi:
543 10.1029/Jc092ic02p01951, 1987.
- 544 Cota, G. F., and Horne, E. P. W.: Physical Control of Arctic Ice Algal Production, *Mar. Ecol. Prog. Ser.*, 52, 111-121, doi:
545 10.3354/meps052111, 1989.

546 Cota, G. F., and Sullivan, C. W.: Photoadaptation, Growth and Production of Bottom Ice Algae in the Antarctic, *J. Phycol.*,
547 26, 399-411, doi: 10.1111/j.0022-3646.1990.00399.x, 1990.

548 Dalman, L. A., Else, B. G. T., Barber, D., Carmack, E., Williams, W. J., Campbell, K., Duke, P. J., Kirillov, S., and Mundy,
549 C. J.: Enhanced bottom-ice algal biomass across a tidal strait in the Kitikmeot Sea of the Canadian Arctic, *Elem. Sci. Anth.*, 7,
550 doi: <https://doi.org/10.1525/elementa.361>, 2019.

551 Duarte, P., Meyer, A., Olsen, L. M., Kauko, H. M., Assmy, P., Rosel, A., Itkin, P., Hudson, S. R., Granskog, M. A., Gerland,
552 S., Sundfjord, A., Steen, H., Hop, H., Cohen, L., Peterson, A. K., Jeffery, N., Elliott, S. M., Hunke, E. C., and Turner, A. K.:
553 Sea ice thermohaline dynamics and biogeochemistry in the Arctic Ocean: Empirical and model results, *J. Geophys. Res.-*
554 *Biogeosciences*, 122, 1632-1654, doi: 10.1002/2016JG003660, 2017.

555 Duarte, P.: CICE-Consortium/Icepack: Icepack with bottom drag, heat and nutrient turbulent diffusion (Version 1.1). Zenodo.
556 <http://doi.org/10.5281/zenodo.4675021>, (2021a, April 9).

557 Duarte, P.: CICE-Consortium/CICE: CICE with bottom drag, heat and nutrient turbulent diffusion (Version 1.1). Zenodo.
558 <http://doi.org/10.5281/zenodo.4675097>, (2021b, April 9).

559 Duarte, P.: The importance of turbulent ocean-sea ice nutrient exchanges for simulation of ice algal biomass and production
560 with CICE6.1 and Icepack 1.2 - CICE forcing files (Version v1.0) [Data set]. Zenodo. <http://doi.org/10.5281/zenodo.4672176>,
561 2021c.

562 Duarte, P.: The importance of turbulent ocean-sea ice nutrient exchanges for simulation of ice algal biomass and production
563 with CICE6.1 and Icepack 1.2 - model simulations (Version v1.0) [Data set]. Zenodo. <http://doi.org/10.5281/zenodo.4672210>,
564 2021c.

565 Gerland, S., Granskog, M. A., King, J., Rösel, A.: N-ICE2015 Ice core physics: temperature, salinity and density [Data set],
566 Norwegian Polar Institute, <https://doi.org/10.21334/npolar.2017.c3db82e3>, 2017.

567 Gosselin, M., Legendre, L., Demers, S., and Ingram, R. G.: Responses of Sea-Ice Microalgae to Climatic and Fortnightly Tidal
568 Energy Inputs (Manitounuk Sound, Hudson-Bay), *Can. J. Fish. Aquat. Sci.*, 42, 999-1006, doi: 10.1139/f85-125, 1985.

569 Graham, R. M., Rinke, A., Cohen, L., Hudson, S. R., Walden, V. P., Granskog, M. A., Dorn, W., Kayser, M., and Maturilli,
570 M.: A comparison of the two Arctic atmospheric winter states observed during N-ICE2015 and SHEBA, *J. Geophys. Res.-*
571 *Atmospheres*, 122, 5716-5737, doi: 10.1002/2016JD025475, 2017.

572 Graham, R. M., Itkin, P., Meyer, A., Sundfjord, A., Spreen, G., Smedsrud, L. H., Liston, G. E., Cheng, B., Cohen, L., Divine,
573 D., Fer, I., Fransson, A., Gerland, S., Haapala, J., Hudson, S. R., Johansson, A. M., King, J., Merkouriadi, I., Peterson, A. K.,
574 Provost, C., Randelhoff, A., Rinke, A., Rosel, A., Sennechael, N., Walden, V., Duarte, P., Assmy, P., Steen, H., and Granskog,
575 M. A.: Winter storms accelerate the demise of sea ice in the Atlantic sector of the Arctic Ocean, *Sci. Rep.-Uk*, 9, Artn 9222,
576 doi: 10.1038/S41598-019-45574-5, 2019.

577 Granskog, M. A., Fer, I., Rinke, A., and Steen, H.: Atmosphere-Ice-Ocean-Ecosystem Processes in a Thinner Arctic Sea Ice
578 Regime: The Norwegian Young Sea ICE (N-ICE2015) Expedition, *J. Geophys. Res.-Oceans*, 123, 1586-1594, doi:
579 10.1002/2017jc013328, 2018.

580 Hegseth, E. N.: Sub-Ice Algal Assemblages of the Barents Sea - Species Composition, Chemical-Composition, and Growth-
581 Rates, *Polar. Biol.*, 12, 485-496, 1992.

582 Hudson, S. R., Cohen, L., Walden, V.: N-ICE2015 surface meteorology [Data set], Norwegian Polar Institute,
583 <https://doi.org/10.21334/npolar.2015.056a61d1>, 2015.

584 Hudson, S. R., Cohen, L., Walden, V.: N-ICE2015 surface broadband radiation data [Data set], Norwegian Polar Institute,
585 <https://doi.org/10.21334/npolar.2016.a89cb766>, 2016.

586 Hunke, E. C., Lipscomb, W. H., Turner, A. K., Jeffery, N., Elliot, S.: CICE: the Los Alamos Sea Ice Model. Documentation
587 and User's Manual Version 5.1. Los Alamos National Laboratory, USA. LA-CC-06-012, 2015.

588 Ingram, R. G., Osler, J. C., and Legendre, L.: Influence of Internal Wave-Induced Vertical Mixing on Ice Algal Production in
589 a Highly Stratified Sound, *Estuar. Coast. Shelf. S.*, 29, 435-446, doi: 10.1016/0272-7714(89)90078-4, 1989.

590 Jeffery, N., Hunke, E. C., and Elliott, S. M.: Modeling the transport of passive tracers in sea ice, *J. Geophys. Res.-Oceans*,
591 116, Artn C07020, doi:10.1029/2010jc006527, 2011.

592 Jeffery, N., Elliott, S., Hunke, E. C., Lipscomb, W. H., Turner, A. K.: Biogeochemistry of CICE: The Los Alamos Sea Ice
593 Model, Documentation and User's Manual. Zbgc_colpkg modifications to Version 5, Los Alamos National Laboratory, Los
594 Alamos, N. M., 2016.

595 Jin, M., Deal, C. J., Wang, J., Shin, K. H., Tanaka, N., Whitley, T. E., Lee, S. H., and Gradinger, R. R.: Controls of the
596 landfast ice-ocean ecosystem offshore Barrow, Alaska, *Ann. Glaciol.*, 44, 9, 2006.

597 Jin, M., Deal, C., and Jia, W.: A coupled ice-ocean ecosystem model for I-D and 3-D applications in the Bering and Chukchi
598 Seas, *Chinese Journal of Polar Science*, 19, 11, 2008.

599 Krause, J. W., Duarte, C. M., Marquez, I. A., Assmy, P., Fernandez-Mendez, M., Wiedmann, I., Wassmann, P., Kristiansen,
600 S., and Agusti, S.: Biogenic silica production and diatom dynamics in the Svalbard region during spring, *Biogeosciences*, 15,
601 6503-6517, doi: 10.5194/bg-15-6503-2018, 2018.

602 Lake, R. A., Lewis, E. L.: Salt rejection by sea ice during growth, *J. Geophys. Res.*, 75, 583-597, 1970.

603 Lannuzel, D., Tedesco, T., van Leeuwe, M., Campbell, K., Flores, H., Delille, B., Miller, L., Stefels, J., Assmy, P., Bowman,
604 J., Brown, K., Castellani, G., Chierici, M., Crabeck, O., Damm, E., Else, B., Fransson, A., Fripiat, F., Geilfus, N. X., Jacques,
605 C., Jones, E., Kaartokallio, H., Kotovitch, M., Meiners, K., Moreau, S., Nomura, D., Peeken, I., Rintala, J. M., Steiner, N.,
606 Tison, J. L., Vancoppenolle, M., Van der Linden, F., Vichi, M. and Wongpan, P.: The future of Arctic sea-ice biogeochemistry
607 and ice-associated ecosystems, *Nat. Clim. Change* 10(11), 983-992, doi: <https://doi.org/10.1038/s41558-020-00940-4>, 2020.

608 Lavoie, D., Denman, K., and Michel, C.: Modeling ice algal growth and decline in a seasonally ice-covered region of the
609 Arctic (Resolute Passage, Canadian Archipelago), *J. Geophys. Res.-Oceans*, 110, Artn C11009, doi: 10.1029/2005jc002922,
610 2005.

611 Leu, E., Mundy, C. J., Assmy, P., Campbell, K., Gabrielsen, T. M., Gosselin, M., Juul-Pedersen, T., and Gradinger, R.: Arctic
612 spring awakening - Steering principles behind the phenology of vernal ice algal blooms, *Progr. Oceanogr.*, 139, 151-170, doi:
613 10.1016/j.pocean.2015.07.012, 2015.

614 Lim, S. M., Moreau, S., Vancoppenolle, M., Deman, F., Roukaerts, A., Meiners, K. M., Janssens, J., and Lannuzel, D.: Field
615 Observations and Physical-Biogeochemical Modeling Suggest Low Silicon Affinity for Antarctic Fast Ice Diatoms, *J Geophys*
616 *Res-Oceans*, 124, 7837-7853, 10.1029/2018jc014458, 2019.

617 Mann, K. H., Lazier, J. R. N.: *Dynamics of Marine Ecosystems*, Third Edition, Blackwell Publishing Ltd., Carlton, Victoria
618 3053, Australia, 503p., doi:10.1002/9781118687901, 2005.

619 McPhee, M.: *Air-ice-ocean interaction: Turbulent ocean boundary layer exchange processes*. Springer-Verlag, New York,
620 216p., doi: 10.1007/978-0-387-78335-2, 2008.

621 McPhee, M. G., Morison, J. H., and Nilsen, F.: Revisiting heat and salt exchange at the ice-ocean interface: Ocean flux and
622 modeling considerations, *J. Geophys. Res.-Oceans*, 113, Artn C06014, doi: 10.1029/2007jc004383, 2008.

623 Mortenson, E., Hayashida, H., Steiner, N., Monahan, A., Blais, M., Gale, M. A., Galindo, V., Gosselin, M., Hu, X. M., Lavoie,
624 D., and Mundy, C. J.: A model-based analysis of physical and biological controls on ice algal and pelagic primary production
625 in Resolute Passage, *Elem. Sci. Anth.*, 5, Artn 39, doi:10.1525/Elementa.229, 2017.

626 Nelson, D. M., and Treguer, P.: Role of Silicon as a Limiting Nutrient to Antarctic Diatoms - Evidence from Kinetic-Studies
627 in the Ross Sea Ice-Edge Zone, *Mar. Ecol. Prog. Ser.*, 80, 255-264, doi: 10.3354/meps080255, 1992.

628 Niedrauer, T. M., and Martin, S.: Experimental-Study of Brine Drainage and Convection in Young Sea Ice, *J. Geophys. Res.-*
629 *Oceans*, 84, 1176-1186, doi: 10.1029/JC084iC03p01176, 1979.

630 Notz, D., and Worster, M. G.: Desalination processes of sea ice revisited, *J Geophys Res-Oceans*, 114, Artn C05006, doi:
631 10.1029/2008jc004885, 2009.

632 Olsen, L. M., Laney, S. R., Duarte, P., Kauko, H. M., Fernández-Méndez, M., Mundy, C. J., Rösel, A., Meyer, A., Itkin, P.,
633 Cohen, L., Peeken, I., Tatarek, A., Róžańska, M., Wiktor, J., Taskjelle, T., Pavlov, A. K., Hudson, S. R., Granskog, M. A.,
634 Hop, H., and Assmy, P.: The seeding of ice-algal blooms in Arctic pack ice: the multiyear ice seed repository hypothesis, *J*
635 *Geophys Res-Biogeosciences*, 122(7), 1529-1548, doi: 10.1002/2016jg003668, 2017.

636 Olsen, L. M., Duarte, P., Peralta-Ferriz, C., Kauko, H. M., Johansson, M., Peeken, I., Róžańska-Pluta, M., Tatarek, A., Wiktor,
637 J., Fernández-Méndez, M., Wagner, P. M., Pavlov, A. K., Hop, H., and Assmy, P.: A red tide in the pack ice of the Arctic
638 Ocean, *Sci Rep*, 9, 9536, 10.1038/s41598-019-45935-0, 2019.

639 Peterson, A. K., Fer, I., Randelhoff, A., Meyer, A., Håvik, L., Smedsrud, L. H., Onarheim, L., Muilwijk, M., Sundfjord, A.,
640 McPhee, M. G.: N-ICE2015 Ocean turbulent fluxes from under-ice turbulence cluster (TIC) [Data set], Norwegian Polar
641 Institute, <https://doi.org/10.21334/npolar.2016.ab29f1e2>, 2016.

642 Reeburgh, W. S.: Fluxes Associated with Brine Motion in Growing Sea Ice, *Polar Biol.*, 3, 29-33, doi: 10.1007/Bf00265564,
643 1984.

644 Rinke, A., Maturilli, M., Graham, R. M., Matthes, H., Handorf, D., Cohen, L., Hudson, S. R., and Moore, J. C.: Extreme
645 cyclone events in the Arctic: Wintertime variability and trends, *Environ. Res. Letters*, 12, Artn 094006, doi:10.1088/1748-
646 9326/Aa7def, 2017.

647 Smith, R. E. H., Cavaletto, J. F., Eadie, B. J., and Gardner, W. S.: Growth and Lipid-Composition of High Arctic Ice Algae
648 during the Spring Bloom at Resolute, Northwest-Territories, Canada, *Mar. Ecol. Prog. Ser.*, 97, 19-29, doi:
649 10.3354/meps097019, 1993.

650 Takeda, S.: Influence of iron availability on nutrient consumption ratio of diatoms in oceanic waters, *Nature*, 393, 774-777,
651 doi: 10.1038/31674, 1998.

652 Tedesco, L., Vichi, M.: BFM-SI: a new implementation of the Biogeochemical Flux Model in sea ice. in: CMCC Research
653 Papers, <http://www.cmcc.it/publications-meetings/publications/researchpapers/rp0081-ans-03-2010>,
654 <http://hdl.handle.net/2122/5956>, 2010.

655 Tedesco, L., Vichi, M., and Scoccimarro, E.: Sea-ice algal phenology in a warmer Arctic, *Sci. Adv.*, 5, ARTN eaav4830, doi:
656 10.1126/sciadv.aav4830, 2019.

657 Thomas, M., Vancoppenolle, M., France, J. L., Sturges, W. T., Bakker, D. C. E., Kaiser, J., and von Glasow, R.: Tracer
658 Measurements in Growing Sea Ice Support Convective Gravity Drainage Parameterizations, *J Geophys Res-Oceans*, 125,
659 ARTN e2019JC015791, doi: 10.1029/2019JC015791, 2020.

660 Turner, A. K., Hunke, E. C., and Bitz, C. M.: Two modes of sea-ice gravity drainage: A parameterization for large-scale
661 modeling, *J. Geophys. Res.-Oceans*, 118, 2279-2294, doi: 10.1002/jgrc.20171, 2013.

662 Urrego-Blanco, J. R., Urban, N. M., Hunke, E. C., Turner, A. K., and Jeffery, N.: Uncertainty quantification and global
663 sensitivity analysis of the Los Alamos sea ice model, *J. Geophys. Res.-Oceans*, 121, 2709-2732, doi: 10.1002/2015JC011558,
664 2016.

665 Vancoppenolle, M., Bitz, C. M., and Fichefet, T.: Summer landfast sea ice desalination at Point Barrow, Alaska: Modeling
666 and observations, *J. Geophys. Res.-Oceans*, 112, Artn C04022, doi: 10.1029/2006jc003493, 2007.

667 Vancoppenolle, M., Goosse, H., de Montety, A., Fichefet, T., Tremblay, B., and Tison, J. L.: Modeling brine and nutrient
668 dynamics in Antarctic sea ice: The case of dissolved silica, *J Geophys Res-Oceans*, 115, Artn C02005, doi:
669 10.1029/2009jc005369, 2010.

670 Vancoppenolle, M., Bopp, L., Madec, G., Dunne, J., Ilyina, T., Halloran, P. R., and Steiner, N.: Future Arctic Ocean primary
671 productivity from CMIP5 simulations: Uncertain outcome, but consistent mechanisms, *Global Biogeochem Cy*, 27, 605-619,
672 doi: 10.1002/gbc.20055, 2013.

673 van Leeuwe, M. A., Tedesco, L., Arrigo, K. R., Assmy, P., Campbell, K., Meiners, K. M., Rintala, J. M., Selz, V., Thomas,
674 D. N. and Stefels, J.: Microalgal community structure and primary production in Arctic and Antarctic sea ice: A synthesis.
675 *Elem. Sci. Anth.*, 6:4., doi: <https://doi.org/10.1525/elementa.267>, 2018.

676 Wakatsuchi, M., and Ono, N.: Measurements of Salinity and Volume of Brine Excluded from Growing Sea Ice, *J. Geophys.*
677 *Res.-Oceans*, 88, 2943-2951, doi: 10.1029/JC088iC05p02943, 1983.

678 Webster, M. A., Rigor, I. G., Nghiem, S. V., Kurtz, N. T., Farrell, S. L., Perovich, D. K. and Sturm, M.: Interdecadal changes
679 in snow depth on Arctic sea ice, *J. Geophys. Res.-Oceans* 119(8), 5395-5406, doi:10.1002/2014JC009985, 2014.

680 Wells, A. J., Wettlaufer, J. S., and Orszag, S. A.: Brine fluxes from growing sea ice, *Geophys Res Lett*, 38, Artn L04501, doi:
681 10.1029/2010gl046288, 2011.
682
683
684
685
686
687